DEVELOPMENT OF COMPACT TIME-DOMAIN TERAHERTZ SPECTROMETER USING ELECTRO-OPTIC DETECTION METHOD

A THESIS SUBMITTED TO
THE GRADUATE SCHOOL OF NATURAL AND APPLIED SCIENCES
OF
MIDDLE EAST TECHNICAL UNIVERSITY

BY

MUKADDES MELİZ METBULUT

IN PARTIAL FULFILLMENT OF THE REQUIREMENTS
FOR
THE DEGREE OF MASTER OF SCIENCE
IN
PHYSICS

SEPTEMBER 2009

Approval of the thesis

DEVELOPMENT OF COMPACT TIME-DOMAIN TERAHERTZ SPECTROMMETER USING ELECTRO-OPTIC DETECTION METHOD

submitted by **MUKADDES MELİZ METBULUT** in partial fulfillment of the requirements for the degree of **Master of Science in Physics Department, Middle East Technical University** by,

Prof. Dr. Canan Özgen
Dean, Graduate School of **Natural and Applied Sciences** _____

Prof. Dr. Sinan Bilikmen
Head of Department, **Physics** _____

Assist. Prof. Dr. Hakan Altan
Supervisor, **Physics Dept., METU** _____

Examining Committee Members:

Prof. Dr. Sinan Bilikmen
Physics Dept., METU _____

Assist. Prof. Dr. Hakan Altan
Physics Dept., METU _____

Dr. Halil Berberoğlu
Physics Dept., METU _____

Dr. Demiral Akbar
Physics Dept., METU _____

Assist. Prof. Dr. Fatih Ömer İlday
Physics Dept., BİLKENT _____

Date:11.09.2009

I hereby declare that all information in this document has been obtained and presented in accordance with academic rules and ethical conduct. I also declare that, as required by these rules and conduct, I have fully cited and referenced all material and results that are not original to this work.

Name, Last name: MUKADDES MELİZ METBULUT
Signature :

ABSTRACT

DEVELOPMENT OF COMPACT TERAHERTZ TIME-DOMAIN TERAHERTZ SPECTROMETER USING ELECTRO-OPTIC DETECTION METHOD

Metbulut, Mukaddes Meliz

M.Sc., Department of Physics

Supervisor: Assist. Prof. Dr. Hakan Altan

September 2009, 81 pages

The goal of this thesis is to describe development of compact terahertz time-domain spectrometer driven by a mode-locked Ti:Sapphire laser. The terahertz radiation was generated by photoconductive antenna method and detected by electro-optic detection method. In this thesis, several terahertz generation and detection method, working principle of terahertz time-domain spectroscopy and its applications are discussed. We mainly focused on working principle of terahertz time-domain spectroscopy and characterization of detected terahertz power using electro-optic detection method.

Keywords: Terahertz Radiation, Terahertz Time Domain Spectroscopy, Terahertz Power, Electro-Optic Detection Method.

ÖZ

ELEKTRO-OPTİK BELİRLEME YÖNTEMİ İLE KOMPAKT ATILIMLI TERAHERTZ SPEKTROMETRE GELİŞTİRİLMESİ

Metbulut, Mukaddes Meliz
Yüksek Lisans, Fizik Bölümü
Tez Yöneticisi: Yar. Doç. Dr. Hakan Altan

Eylül 2009, 81 sayfa

Bu tezin amacı Ti:Safir lazerle sürülmüş kompakt atılımlı terahertz spektrometre geliştirmesidir. Terahertz ışınları fotoiletken anten metoduyla üretilip elektro-optik belirleme yöntemiyle algılanmıştır. Bu tezde birçok terahertz üretme ve algılama yöntemleri, kompakt atılımlı terahertz spektometresinin çalışma prensipleri ve uygulamaları tartışılmıştır. Esas olarak kompakt atılımlı terahertz spektometresinin çalışma prensiplerine ve belirlenen terahertz gücünün karakterizasyonuna odaklanılmıştır.

Anahtar Kelimeler: Terahertz, Kompakt Atılımlı Terahertz Spektroskopisi, Terahertz Gücü, Elektro-Optik Belirleme Yöntemi.

to my lovely family...

ACKNOWLEDGEMENTS

I would like to thank to my supervisor Assist. Prof. Dr. Hakan Altan for his support and guidance. His valuable comments, criticism and suggestions had great contribution to this work. Furthermore, I would like to thank to the rest of my thesis committee; Prof. Dr. Sinan Bilikmen, Dr. Halil Berberoğlu, Dr. Demiral Akbar and Assist. Prof. Dr. Fatih Ömer İlday for their contribution and valuable comments.

I would like to express my gratitude to my laboratory partners Ümmügül Erözbek Güngör and Hasan Hüseyin Güllü for their productive team work, support and friendship. Also I would like to thank to other group members Zahide Tosun and Dr. Halil Berberoğlu for their friendship and support.

Finally I express my deepest gratitude to my sister, Pınar, my mother, Cansev, and my father, Mustafa Metbulut for their continuous support and endless love. I would like to express special thanks to my mother and my grandmother, Mukaddes Özgün, for always supporting me and teaching a lot throughout my life. It couldn't be possible to complete this thesis without them.

TABLE OF CONTENTS

LIST OF TABLES

TABLES

LIST OF FIGURES

FIGURES

LIST OF SYMBOLS AND ABBREVIATION

BS: Beam Splitter

CC: Corner Cube

CdTe: Cadmium Telluride

CO: Carbon Monoxide

CO_2: Carbon Dioxide

eV: Electron Volt

FEL: Free Electron Laser

fs: Femtosecond

GaAs: Gallium Arsenide

GaSe: Gallium Selenide

GaP: Gallium Phosphide

HCl: Hydrogen Chloride

HMX: cyclo-tetramethylene tetranitramine

H_2O: Water

Hz: Hertz

InAs: Indium Arsenide

InP: Indium Phosphide

InSb: Indium Antimonide

kHz: Kilohertz

$LiNbO_3$: Lithium Niobate

M: Mirror

meV: mili electron Volt

MHz: Megahertz

NLTL: Nonlinear transmission line

O_2: Dioxide

O_3: Trioxide

OBJ: Objective

PbTe: Lead Telluride

PCA: Photoconductive Antenna

PD: Photodetector

PM: Parabolic Mirror

PTN: pentaerythritol tetranitrate

ps: Picosecond

QCL: Quantum Cascade Laser

QP: Quarter Wave Plate

RDX: cyclo-1,3,5-trimethylene

SO_2: Sulfide Dioxide

Te: Tellurium

THz: Terahertz

THz TDS: Terahertz Time-Domain Spectroscopy

Ti:Al_2O_3: Titanium Sapphire

Ti:Sapphire: Titanium Sapphire

TNT: 2,4,6-trinitrotuelene

TO: Transverse Optical

WP: Wollaston Prism

ZnTe: Zinc Telluride

CHAPTER 1

INTRODUCTION

1.1 TERAHERTZ WAVES

Terahertz region of electromagnetic spectrum has become very popular recently. It is located between microwave and far-infrared regions forming a bridge between electronics and photonics. This multidisciplinary character of terahertz radiation makes it very important and attractive. Although the electronics and photonics are two well-developed areas, terahertz radiation residing along their borders is an unexplored part of electromagnetic spectrum containing lots of information. THz region, which is also known as far-infrared radiation or T-rays, covers the frequency band of electromagnetic spectrum between 0.1 and 10 THz. 1 terahertz corresponds to a wavelength of 300 μm and encompasses energy of approximately 4 meV. The position of terhertz waves in electromagnetic spectrum is shown in the figure 1.1.

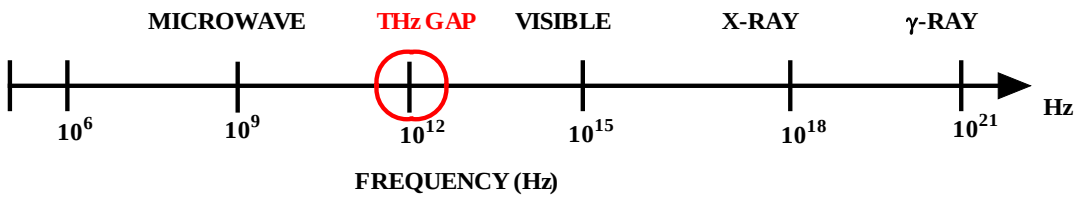

Figure 1.1: Electromagnetic spectrum.

There are four main properties of terahertz waves that make them very attractive and important. Firstly, terahertz radiation has unique signature for different materials. Many organic molecules show strong absorption and dispersion due to their vibrational and rotational transitions that fall directly to THz region. Moreover terahertz radiation can be used to determine lattice vibrations and free carrier absorption in dielectrics. Secondly, terahertz radiation can pass through most non-metallic and non-polar materials but strongly interacts with polar materials. So polar molecules such as H_2O, HCl, O_3, CO and SO_2 have unique spectral peaks in their absorption spectra in THz region providing a signature of these molecules. This signature of molecules in terahertz radiation provides a significant application to determine and identify the properties of a particular medium. So THz radiation can be used to detect air pollution, presence of a particular gas, skin cancer (cancer cells contain more water than normal cells) and explosive material. Thirdly, terahertz regime encompasses very low energies such as few meV and due to this reason; they do not cause any ionization in biological tissues. Hence it is not harmful for people [1-2]. Moreover, because of its nondestructive and noninvasive inspection of matter it is well suited for security and medical applications. Fourthly, an object at room temperature emits energy in THz region. Furthermore, 98% of photons emitted since Big Bang fall into the far infrared and submilimeter region [3].

Natural source of terahertz radiation is black body radiation. Since it is based on thermal emission from object, it is incoherent and very weak. The intensity versus frequency graph in figure 1.2 indicates weakness of the power of emitted terahertz radiation at 300 K.

Terahertz science remained unexplored until the beginning of the 90's due to lack of available generation and detection method for terahertz radiation. Only at that time methods for both detection and generation are developed and subsequently coherent radiation is obtained. The coherent terahertz radiation sources can be classified as continuous and pulsed. In this thesis, several methods of both generation and detection of terahertz radiation are discussed.

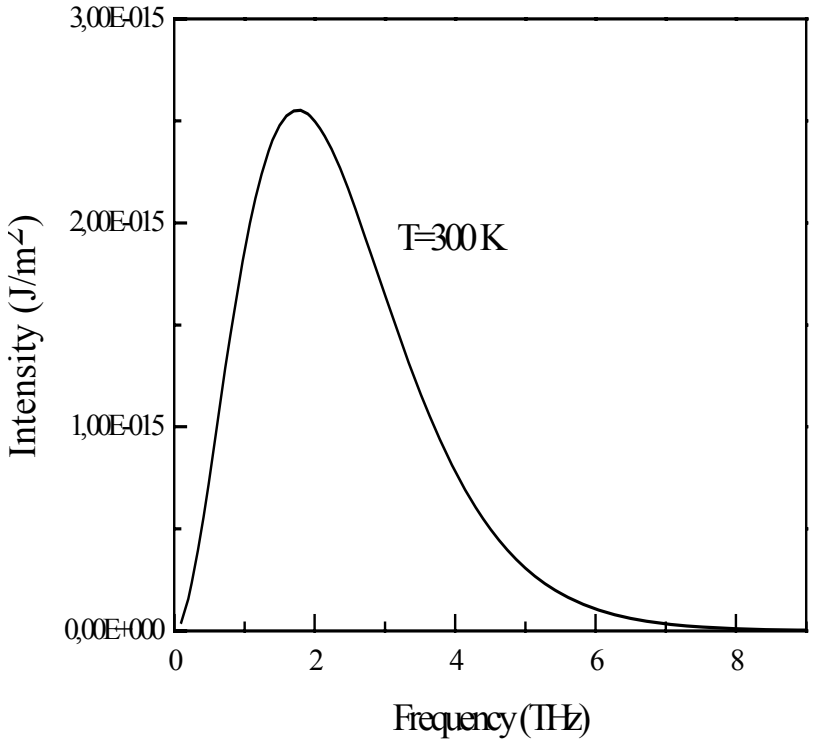

Figure 1.2: Intensity of blackbody radiation at 300 K.

1.2 TERAHERTZ RADIATION SOURCES

After the development of the terahertz generators, there has been a great deal of interest in terahertz science. These generators involve both coherent and incoherent sources. Mercury arc lamp is an example of an incoherent terahertz radiation source [4]. Both the continuous and pulsed coherent radiation sources are discussed in the following subsections.

1.2.1 CONTINUOUS TERAHERTZ RADIATION

Other than Terahertz time-domain spectroscopy for analysis of atoms or molecules, continuous terahertz sources are used in order to obtain high spectral resolution. The terahertz sources in question are namely photomixers [5-7], backward wave oscillators [8], free electron lasers [9-10], gas lasers [8-11] and quantum cascade lasers [12-15].

In photomixers, terahertz radiation is obtained through photomixing process. The photomixing, also known as optical heterodyne down conversion, is based on optical down conversion from optical frequencies and it is obtained by focusing two single-mode continuous wave laser beams onto the photomixer. Mixing the two continuous laser pulses at different frequencies creates an optical beat generating continuous terahertz radiation at beat frequency. It is also possible to tune over the terahertz band by shifting the optical frequency of one of the lasers used. Disadvantage of photomixer terahertz source is that the generated terahertz power is limited by thermal damage threshold and low compared to the other continuous wave sources, which are in the microwatt range. In addition, its optical to terahertz inversion efficiency is low between 10^{-6} and 10^{-5} [7].

There are also free electron based sources of continuous terahertz radiation including backward wave oscillators [16] and free electron lasers [9-10]. The backward wave oscillator is a slow wave device operating in power range between 1 and 100 mW. On the other hand, free electron lasers are able to provide nearly 20 W power. The terahertz emission mechanism of free electron laser relies on synchrotron radiation. One method is that after the semiconductor material of the free electron laser is excited with a pumping laser, a bunch of free electrons are created by photoemission. These electrons are accelerated by magnetic field until they attain relativistic energies of the synchrotron radiation. Another method uses electron gun to generate the electron beams. In the electron gun, laser light is incident on a cathode and electrons are generated by means of photoelectric effect.

The other alternative sources of continuous terahertz radiation are gas lasers. These gases are pumped with CO_2 laser in order to excite gas molecules. The most commonly used gas is methanol due to its emission at 118 μm (2.54 THz) with about 100 mW emitted power [8].

Another way to generate terahertz radiation is using quantum cascade laser (QCL). Although quantum cascade lasers are still under development, they have great effect on terahertz technology since they are compact and able to produce power in miliwatt range. However, QCLs are yet not able to work at room temperature and cooling is necessary for them at least to liquid nitrogen temperatures [13]. When compared to other semiconductor lasers, their working principle is different. In contrary to other semiconductor lasers in quantum cascade laser the conduction band is split into distinct repeating subbands, multiple quantum wells, by quantum confinement. To excite intersubband transitions electrons are injected to through the quantum wells under an applied bias. As a result they undergo intersubband transitions and subsequently emit terahertz radiation. Since excitation occurs through multiple quantum wells, emission occurs in a cascaded manner.

1.2.2 PULSED TERAHERTZ RADIATION

Either nonlinear crystals that make use of the nonlinear optical response of bounded electrons or semiconductors that use the transient current induced by optical femtosecond pulses give rise to pulsed terahertz radiation. The most widely used two methods for obtaining pulsed terahertz radiation are photoconductive antenna methods [17-19] and optical rectification methods [20-26]. In addition to these two sources, there are several ways to generate pulsed terahertz radiation including semiconductor quantum structures, coherent longitudinal optical phonons, high temperature superconducting bridges, surge current at surface of semiconductors and electronic devices.

The photoconductive antenna is a semiconductor structure in which two metal electrodes are deposited onto a semiconductor substrate. The distance between the electrodes ranges from few μm to several mm [27]. The schematic description of the antenna structure is shown in figure 1.3.

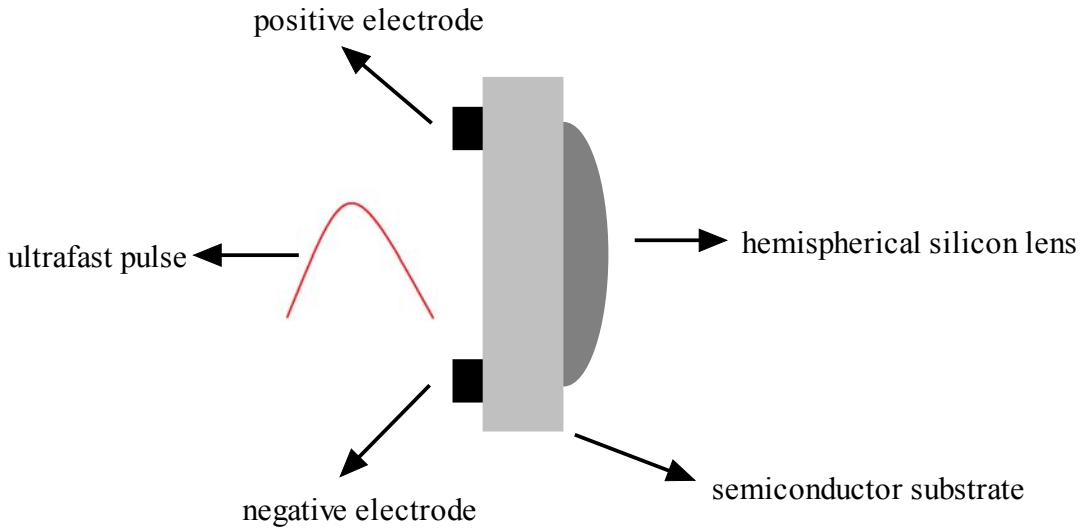

Figure 1.3: Schematic structure of a photoconductive antenna.

Auston generated terahertz pulses with a photoconductive antenna for the first time in 1984 [28]. In photoconductive antenna method illuminating the biased photoconductive antenna with a femtosecond laser generates terahertz radiation. The laser light incident on the gap between the electrodes generates free electron hole pairs in the semiconductor. Applying a DC voltage directs these free charge carriers that gives rise to transient photocurrent that is to say time varying current, which is the origin of terahertz radiation emission. Hence, the electric field of the emitted terahertz pulse is related to the change in transient photocurrent by,

$$E_{THz} \propto \frac{\partial J(t)}{\partial t} \tag{1.1}$$

This process occurs in case the photon energy of the laser pulse is greater than or equals to the band gap energy of the semiconductor material. Hence, terahertz generation from photoconductive antenna is a resonant process indicating that terahertz pulse width is limited by the response time of the material. Therefore, semiconductor material of the photoconductive antenna must have rapid photocurrent rise time in order to obtain efficient terahertz emission. Typically, low temperature grown GaAs is used for photoconductive antennas, which has carrier lifetime of 200-500 fs. The other important property of the semiconductor material is its breakdown field since it determines the maximum applicable bias voltage value.

In contrary to generation from photoconductive antenna, optical rectification [29] in a nonlinear crystal is a non-resonant process. Because of this, THz pulse width only depends on the laser pulse width and the phonon mode absorptions of the crystal. Optical rectification is defined as the inverse of the electro-optic effect [30] and it is first observed in 1970's using $LiNbO_3$ crystal producing far infrared pulses [31]. In this generation, method femtosecond laser light is focused on a nonlinear crystal and difference frequency, or mixing process occurs. Subsequently terahertz emission occurs. Since the difference frequency mixing is a second order nonlinear process, terahertz emission depends on the value of the second order electrical susceptibility of the crystal used. In this nonlinear process, electric field of the pump beam establishes a polarization in the crystal that is related to its second order electric susceptibility.

$$P^{(2)}(t) \propto \chi^{(2)} E(t)^2 \tag{1.2}$$

The formula (1.2) indicates that signal strength is linearly proportional to the intensity of the pump beam and the second order electro-optic tensor of the nonlinear crystal. Therefore, crystals having high second order electro-optic tensors are favorable for optical rectification. Most widely used crystal for optical rectification is ZnTe in spite of its drawbacks. For instance, there are other processes including two-photon absorption and second harmonic generation competing with

optical rectification [32]. In addition, it has phonon resonance at 5.3 THz preventing the terahertz emission at this range.

There are some conditions to be met to achieve optical rectification. First of all phase matching condition must be satisfied to rectify terahertz pulses that is to say phase velocity of the terahertz pulse and group velocity of the laser pulse must be matched [29, 33-35]. Secondly, material of the crystal used must be transparent at terahertz and optical frequencies.

When the optical rectification method is compared the photoconductive antenna method it has both weakness and superiority. Its weakness is that the generated signal with photoconductive antenna is about hundred times more powerful than that of the nonlinear crystals because of the low efficiency in conversion of the optical frequencies to terahertz frequencies. On the other hand, nonlinear crystal can provide a wide spectrum up to 51 THz whereas the photoconductive antennas provide a spectrum of few terahertz [36-37].

The other alternative source for terahertz radiation is coherent longitudinal optical phonons [38-40]. Pumping semiconductors with femtosecond pulses gives rise to terahertz emission by creating optical phonons instead of optical rectification method. Femtosecond optical pulses incident on a semiconductor surface causes excitation of carriers that creates an electrical transient. The excitation mechanism is based on either the ultrafast screening of the surface depletion field or ultrafast building up of photo-Dember field. In both mechanisms, the created electrical transient initiates coherent lattice vibrations, which emit terahertz waves. Longitudinal optical phonons are directed normal to the surface so their effective charge density is not zero. Thus, they induce macroscopic polarization that emits terahertz radiation at the longitudinal optical phonon frequency. On the other hand effective charge density of transverse optical phonons is zero, thus they cannot induce a macroscopic polarization that emits terahertz radiation. However, in general longitudinal optical phonons do not interact with electromagnetic waves since they are transverse waves. Nevertheless, when the wave vector q is exactly zero longitudinal and transverse modes are degenerate and

cannot be distinguished [41]. Therefore, at zero wave number longitudinal optical phonons can interact with electromagnetic waves. This was first theoretically predicted in GaAs [39] and first experimentally observed in Te [42]. Later also observed in GaAs [43], PbTe and CdTe [44]. Furthermore, terahertz radiation is also obtained from longitudinal optical phonon-plasmon coupling in InSb films where wave vector q is zero [45].

The other way of having terahertz radiation from semiconductors is the surge current at semiconductor surface induced by photoexcitation [46]. The acceleration of photoexcited carriers by the surface depletion field and the photo-Dember effect arising from the difference between the diffusion velocities of the electrons and holes and subsequent relaxation of the charge distribution are two proposed mechanism for the origin of the induced surge current [47]. In both generation mechanisms increase in the induced surge current is proportional to the laser pulse duration. Surge current induced in a wide bandgap semiconductor is explained by the effect of the surface depletion field while in a narrow bandgap semiconductor it is explained by the photo-Dember effect [48]. It is possible to determine the dominant mechanism that creates surge current by comparing the polarity of the emitted terahertz radiation in p-type and n-type semiconductor. In the mechanism, originating from photo-Dember effect polarity of the terahertz radiation is same regardless of the type of the semiconductor. The reason for this is that the direction of the diffusion current is same for both types of semiconductors since the mobility of electrons are higher than that of the holes. On the other hand in the other mechanism polarity of the emitted terahertz radiation is opposite for n-type and p-type semiconductors since the direction of the depletion field is opposite for n-type and p-type semiconductors. In semiconductors such as InSb, InAs [49] and GaAs [50] the dominant mechanism is photo-Dember effect whereas in InP [47] it is surface depletion field.

On the other hand semiconductor quantum structures are alternative sources where excitonic charge oscillations emit terahertz beams. This emission is observed in both double-coupled quantum well [51] and single quantum well structures [52]. Coherent optical excitation of light and heavy hole excitons in quantum wells generate charge

oscillations resulting from the time evolution of light and heavy hole exciton states. Consequently light hole and heavy hole valence band mixing gives rise to a time varying dipole moment, emitting terahertz radiation.

Furthermore, terahertz radiation is obtained from high critical temperature superconductors. Emission of terahertz waveform is based on the modulation of the superconductor with optical femtosecond pulses, which is observed in $YBa_2Cu_3Y_{7-\delta}$ thin films [53].

In addition to the aforementioned sources, nonlinear transmission lines are another alternative for electrical generation of terahertz radiation. Nonlinear transmission line (NLTL) is a transmission line loaded with reverse biased diodes functioning as voltage variable capacitors that triggers a voltage dependent velocity for the wave propagating through it. To obtain far infrared radiation the NLTL is coupled to a bow tie antenna [54].

1.2.2.1 TERAHERTZ TIME DOMAIN SPECTROSCOPY

Terahertz time domain spectroscopy is a technique to obtain spectroscopic analysis in time domain and with its Fourier transform in frequency domain. Its advantage over other methods is that it measures electric field at terahertz frequencies. The measurement of electric field not only provides information on amplitude but also phase. In this respect it is superior to conventional Fourier transform spectroscopy that measures only intensity. The other advantage of this spectroscopy is determination of real and imaginary parts of refractive index without making calculations using Kramers-Kronig relations. Experiment in this method can be carried out either by reflection or transmission geometry. However, transmission geometry is more prevalent due to its easier alignment.

1.3 TERAHERTZ DETECTORS

Three basic detectors for terahertz radiation are photoconductive antennas, electro-optic crystals and bolometers. Among these three photoconductive antennas and electro-optic crystals are more popular. In this thesis, emphasis will be given on electro-optic detection method.

Auston first demonstrated detection of terahertz pulses by photoconductive antennas in 1984 [28]. In case the carrier lifetime of the photoconductive antenna is shorter than the terahertz pulse, the antenna works as a gate that samples the terahertz waveform. Detection method is based on opposite mechanism of the generation method with antenna. After both the terahertz beam and the probe beam are also focused on the photoconductive antenna, it is gated with a femtosecond optical pulse that creates free charge carriers. Electric field of the terahertz beam acts as a bias field in the antenna to accelerate the generated free charge carriers. Subsequently current proportional to the electric field of the incoming terahertz pulse is created. Therefore, detected current gives information about the terahertz beam. Detection is achieved by varying the time delay between the optical pulse and the terahertz pulse. Different limiting factors affect the detection bandwidth of the photoconductive antenna [19]. There are two dominating factors: one is its resonant property and the other is its carrier lifetime. Former is due to the geometry of the antenna while the latter one is due to the property of substrate material. The carrier life time imposes upper frequency limit for detection. However it is shown experimentally that photoconductive antennas can detect up to 40 THz when they are gated with ultra short pulses as short as 15 fs [55].

The other terahertz detector is bolometer. In fact, it is based on thermal detection and limited in its application [56-57] because it can only measure the total energy of a terahertz pulse, rather than its electrical field. Since they detect thermal radiation they are strongly influenced by the background thermal radiation unless they are cooled. Therefore, they need to be cooled with helium in order to achieve good sensitivity for terahertz detection. This makes them bulky and expensive. Consequently, both the photoconductive antenna and electro-optic detection method, which are time-gated

methods are more favorable than bolometric detection method.

1.3.1 ELECTRO-OPTIC DETECTION METHOD

Wu and Zhang first achieved the electro-optic detection for terahertz radiation in 1995 [58]. Mechanism of electro-optic detection is based on the Pockels effect that is a physical phenomenon referring to a proportional variation in the principal refractive index of an electro-optic crystal at visible and near infrared frequencies with an applied electric field. In this detection method, terahertz electric field acts as the applied electric field. Contrary to antenna detection, it is a non-resonant process signalizing that terahertz radiation is instantaneously sensed in electro-optic detection method. Due to the instantaneous effect of the Pockels effect, electro-optic crystals act as a gate sampling terahertz waveform. As a result, the electric field of terahertz beam simultaneously induces a variation in the refractive index that is denoted as birefringence. In consequence, due to the induced birefringence as the femtosecond optical pulse, it propagates through the crystal simultaneously with terahertz pulse will have a phase modulation. Thus focusing both the terahertz beam and the optical probe beam on the crystal collinearly performs electro-optic detection. In electro-optic detection, what we measure is this induced difference in refractive indices in different axes of the crystal and the subsequent change in the polarization state of the probe beam. The effect of the terahertz beam on the refractive indices of the crystal and the polarization state of the probe beam is illustrated in figure 1.4.

In order to sense the phase modulation in the optical pulse, optical components such as quarter wave plate and Wollaston prism is positioned after the detection crystal. The schematic view of electro-optic detection system is shown in figure 1.5.

The function of quarter wave plate is to convert linearly polarized light into circularly polarized light. In case the light is elliptically polarized light, it does not change the polarization of the light but gives rise to 90° shift in its plane of polarization. In lack of the terahertz beam, the two propagation modes of the optical

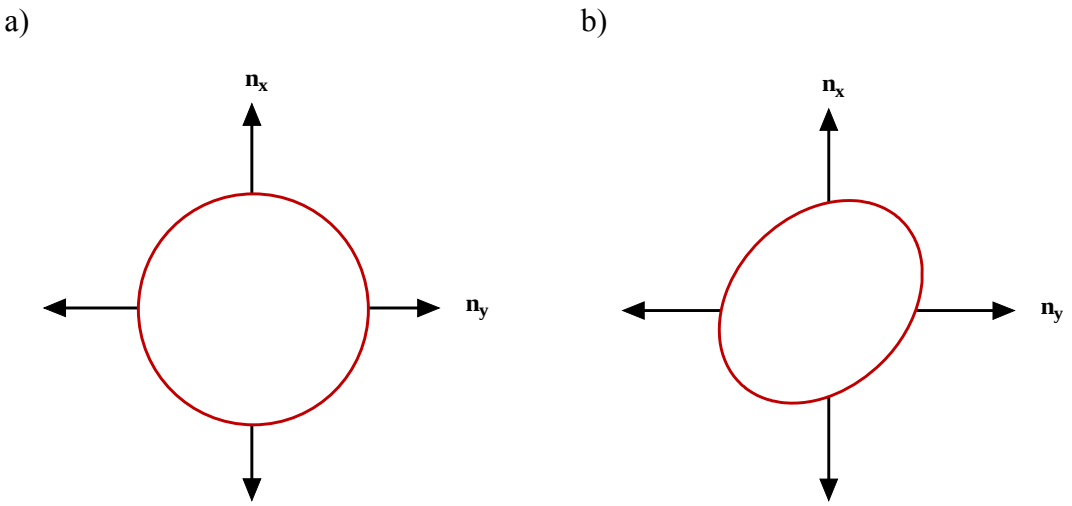

Figure 1.4: Index ellipsoid of the detection crystal a) before the THz beam b) after the THz beam

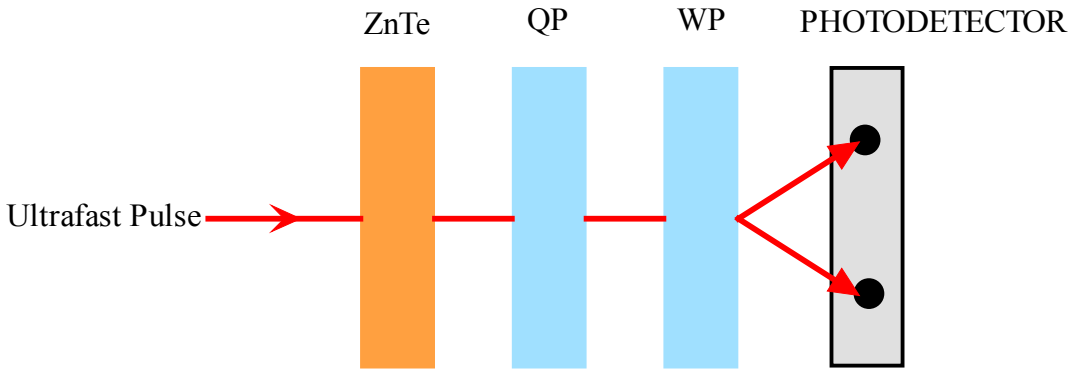

Figure 1.5: Schematic view of electro-optic detection setup.

beam passing through the isotropic detection crystal will be subjected to the same phase retardation. Henceforth optical beam propagating through the quarter wave plate is converted into circularly polarized light. On the contrary, presence of terahertz beam induces a birefringence in the electro-optic crystal so the two modes of the optical beam propagating through it will be subjected to different phase retardation. As a result, the linearly polarized light coming from the crystal will be transformed into elliptically polarized light. The phase retardation between the two propagating modes are given by [59],

$$\Delta\Gamma = \frac{2\pi}{\lambda} n^3 r_{41} L E_{THz} \tag{1.3}$$

where E_{THz} is the electric field of the terahertz radiation, n is refractive index of the crystal at the wavelength of the probe beam, r_{41} is the electro-optic coefficient and L is the length of the crystal respectively.

After the quarter wave plate optical beam is modulated in such a way that indicating either presence or lack of the terahertz electric field. The induced birefringence in the crystal creates a discrepancy in the intensity of the two separated probe beams. In case of the presence of the terahertz beam inside the electro-optic crystal, the intensity of the separated two lights will be different due to the different phase retardation they exposed to. On the contrary, equal intensity is observed in the lack of terahertz electric field since in this case two propagating modes are subjected to the same phase modulation. This intensity difference is detected by a photodiode, which is directly proportional to the terahertz electric field. However in order to be able to sense the intensity values of the two propagating modes of the optical beam individually, it is directed to pass through the Wollaston prism. It is an optical device whose function is separating the incoming light into two orthogonolized linearly polarized light. In order to obtain whole time dependent electric field the delay between the terahertz and probe pulse is varied. By connecting the photodetector to the lock-in amplifier the obtained signal is processed to map out the terahertz waveform.

Detection of terahertz pulses with electro-optic detection method requires some conditions to be met. These requirements can be listed as

i. Crystal used must be transparent to both the terahertz and the optical pulse
ii. Crystal must be non-centrosymmetric and isotropic to detect the induced birefringence
iii. Phase-matching condition between optical and terahertz beam must satisfied

The most widely used electro-optic crystals for electro-optic detection is zinc telluride (ZnTe), gallium selenide (GaSe) and gallium phosphide (GaP). The efficiency of these crystals is rated with the value of their electro-optic coefficient that is listed in table 1. In this thesis, ZnTe crystal is chosen as detection crystal because its refractive index at near infrared and terahertz frequencies is comparable.

Efficient detection of terahertz radiation also depends on the thickness of the crystal and orientation of the polarization of the probe and terahertz beam. Firstly the effect of crystal thickness is also can be seen from the phase retardation formula (1.3). The induced phase retardation in transmitted optical beam is proportional to kL. Therefore, as the crystal thickness increases, the phase retardation induced in the crystal increases too. Consequently, measurement sensitivity increases as the crystal thickness increases. On the other hand, in thin sensor crystals probe beam reflects back from the crystal air interface and makes another sampling to the same terahertz pulse. In addition, frequency bandwidth that depends on the transit time of light in the crystal is inversely proportional to the crystal thickness. Since the refractive index of crystal is different for terahertz and optical beam, they propagate through the crystal with slightly different velocities. As a result of this, group velocity mismatch occurs between the terahertz and the probe beam. Secondly there exist optimum angles between polarizations of terahertz and probe beam providing maximum signal for electro-optic detection [61], which are are 0º and 90º.

Table 1.1: Electro-optic coefficients of terahertz electro-optic detectors [60]

MATERIAL	STRUCTURE	ELECTRO-OPTIC COEFFICIENT (pm/V)
ZnTe	Zincblende	$r_{41} = 3.9$
GaSe	Hexagonal	$r_{41} = 14.4$
GaP	Zincblende	$r_{41} = 0.97$

Several effects cause distortion in detected terahertz waveform such as group velocity mismatch between terahertz and probe beam, absorption and dispersion of terahertz beam in electro-optic crystal [62], phonon-polariton coupling [63] and finite probe pulse width [64]. As mentioned before origin of group velocity mismatch is different propagation speed of the pump and probe beam and this leads to frequency filtering in detection process. The coherence length is given by the formula [34],

$$l_C = \frac{\pi c}{\omega_{THz} \left| n_{opt} - n_{THz} \right|} \tag{1.4}$$

Furthermore photon-polariton coupling occurs as a result of strongly coupling of terahertz pulse to TO-phonon resonance. Consequently terahertz pulse becomes mixed light-polarization states that are called phonon-polaritons. The effect of phonon-polariton coupling on terahertz waveform is an oscillatory tail following the terahertz peak. In addition finite probe pulse width causes weakening and broadening of the detected terahertz waveform.

1.4 APPLICATIONS

Terahertz radiation has characteristic advantages over other radiations. What makes terahertz time-domain so significant are these properties of terahertz radiation. It has extended use in several areas ranging from scientific research to commercial applications. However in this thesis only three major applications are discussed.

1.4.1 MATERIAL CHARACTERIZATION AND SECURITY APPLICATIONS

Terahertz time domain spectroscopy is an effective tool for material characterization. It is of great interest since it has lots of potential applications. One of the applications is identification of an unknown gas by making use of its distinctive absorption spectra [65]. The other applications of material characterization are determination of dielectric function of ferroelectrics [66], complex conductivity of semiconductors [67] and, frequency dependence of surface resistance and conductivity of superconductors [68-69]. Moreover it is possible to identify chemical, biological [70] and explosive agents [71] with their spectral signature. The explosive agents RDX (cyclo-1,3,5-trimethylene), HMX (cyclo-tetramethylene tetranitramine), PETN (pentaerythritol tetranitrate) and TNT (2,4,6-trinitrotuelene) have fingerprints in the THz region [72-73].

1.4.2 BIOLOGICAL AND MEDICAL APPLICATIONS

Applications in biology and medicine arise huge interest. One most significant subject in medicine is designation of basal cell carcinoma, which is known as skin cancer [74-75]. Since tumors have much more water content than that of healthy cells, it is possible to distinguish them. The other medical application is investigation in tooth tissues [76]. Furthermore, applications of terahertz time domain

spectroscopy focus on DNA, RNA and protein diagnostics [77-80]. In addition, most of the vibrational modes of hydroxides fall into terahertz frequencies allowing their identification [81].

1.4.3 IMAGING APPLICATIONS

What makes imaging a very interesting application is the high resolution of terahertz waves (less than 1 mm). Zhang first showed imaging with terahertz time-domain spectroscopy using electro-optic detection in 1996 [82]. Terahertz pulse is able to propagate through clothes, paper and plastic packages while it is reflected back from metals. Therefore it enables inspection of concealed threat substances under barriers. Remote detection of hidden weapons such as knives and guns within clothes or packages is also possible.

1.5 OVERVIEW OF THE THESIS

The goal of this thesis is to address issues such as the development of a compact time domain terahertz spectrometer and investigation of detected terahertz power with electro-optic detection methods. In chapter two, experimental aspects of terahertz time domain is described, which includes detailed information on instrumentation, system design and operation of compact terahertz time-domain spectroscopy. Then in chapter three, detected terahertz power is characterized using electro-optic detection methods. Finally in chapter four, the work is summarized.

CHAPTER 2

COMPACT TERAHERTZ TIME DOMAIN SPECTROMETER

2.1 THz TIME DOMAIN SPECTROSCOPY

Development of terahertz time-domain spectroscopy has opened unexplored but scientifically and technologically important region of electromagnetic spectrum for spectroscopic studies in the beginning of 1990's. Since this spectroscopy is based on generation and detection of picosecond pulses by using femtosecond laser pulses, it became available only after the development of femtosecond lasers. What makes terahertz time domain spectroscopy a powerful experimental tool is direct measurement of electric field to gather information at terahertz frequencies. This allows simultaneous determination of refractive index and absorption coefficient of a sample without need for Kramers-Kronig based calculations.

There are several ways to generate and detect terahertz waves, which were discussed briefly in the first chapter in sections 1.2 and 1.3. In this work photoconductive antenna generation and electro-optic detection methods were used. The pumping femtosecond laser source employed was a Ti:Al_2O_3 mode-locked laser. In this chapter experimental aspects of the terahertz time domain spectrometer is discussed. The schematic diagram of the constructed compact terahertz time domain

spectrometer is shown in figure 2.1.

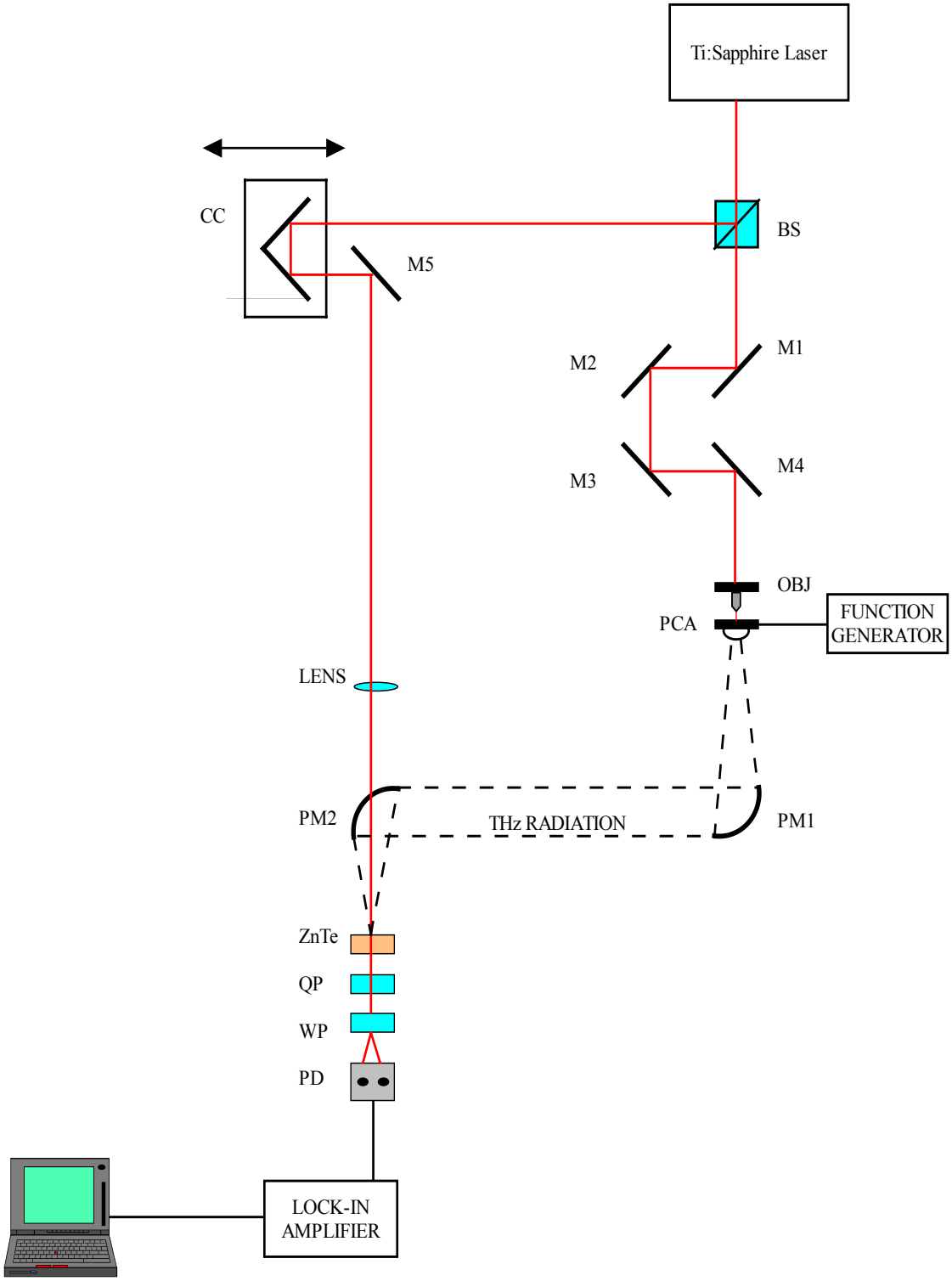

Figure 2.1: Illustration of the compact terahertz time domain spectrometer.

There are two arms in the spectrometer; one is the generation arm where the terahertz radiation is obtained and the other is detection arm where terahertz radiation is detected. Beam splitter divides the laser light into these two arms as pump and probe beams respectively. In generation arm femtosecond laser pulses are directed to an objective in order to focus laser light onto the photoconductive antenna, where the terahertz radiation is generated. After the photoconductive antenna, two parabolic mirrors are positioned to collimate the terahertz beam onto the detection crystal, ZnTe. The probe beam first passes through the corner cube that is positioned on a stepper stage where the time delay between pump and probe beam is obtained. Afterwards, using a lens the probe beam is focused onto the detection crystal. Then the probe beam propagates through the quarter wave plate and Wollaston prism successively. Next a photodetector is positioned behind them to detect the electro-optic signal. Finally the photodetector is connected to a lock-in amplifier, where the signal is processed to map out the terahertz waveform.

2.2 SYSTEM DESIGN AND INSTRUMENTATION

In this section, components of the spectrometer such as femtosecond laser, focusing and collimating optics and, electronic devices such as lock-in amplifier are described.

In our experiments, we used mode-locked Ti-Sapphire ($Ti:Al_2O_3$) laser for both the pump and the probe beam at a center wavelength of 800 nm with pulse duration of 15 fs at 70 MHz repetition rate. The average power of the laser was ~340 mW. Some specifications of the Ti:Sapphire laser are given in table 2.1 [83].

In the generation arm there were four mirrors to create an additional optical path for the pump beam. The aim of additional path is to equate the optical paths of the pump and the probe beam. These four mirrors collimated the laser pulses to the objective, which is an optical element focusing the light to a very small point. The objective

Table 2.1: Specifications of Ti:Sapphire laser [83]

SPECIFICATIONS OF THE LASER	
PULSE DURATION	< 20 fs
SPECTRAL WIDTH	> 40 nm
AVERAGE OUTPUT POWER	> 300 mW
OUTPUT ENERGY AT 75 MHz	> 4 nJ
PUMP BEAM DIAMETER	2 mm ($1/e^2$), TEM_{00}

used in our system was Olympus PLN 20X with 0.4 numerical aperture, 1.2 mm working distance and 22 field number.

Photoconductive antenna was placed just behind the objective. In order to obtain high efficiency photoconductive antenna was positioned very close to the objective considering its 1.2 mm working distance. In our system we used Batop PCA-44-06-10-800 photoconductive antenna. The electrical and optical excitation parameters of the antenna are given in tables 2.2 and 2.3 respectively [84]. The substrate material of this photoconductive antenna is low temperature grown GaAs. It is the most commonly used semiconductor for photoconductive antenna substrates since it shows relatively good carrier mobility. Properties of low temperature grown GaAs are listed in table 2.4. A silicon hemispherical lens mounted on the back side of the antenna is used to efficiently couple the terahertz radiation to free space, since it prevents radiation losses due to reflections at the air-substrate interface. Due to its geometry the lens has no spherical aberration and coma [86]. Furthermore, silicon has very low absorption and a quasi-constant refractive index between 0.2 and 5 THz, which prevents chromatic aberration.

Table 2.2: Electrical parameters of the photoconductive antenna [84]

ELECTRICAL PARAMETERS	
Dark resistance	25 MΩ
Dark current at 10 V	400 nA
Voltage	20 V

Table 2.3: Optical excitation parameters of the photoconductive antenna [84]

OPTICAL EXCITATION PARAMETERS	
Laser excitation wavelength	800 nm
Optical mean power	40 mW
Optical mean power density	100 kW/cm^2
Carrier recovery time	400 fs

Table 2.4: Properties of low temperature grown GaAs [85]

PROPERTIES OF LT-GaAs	
Carrier Lifetime	0,3 ps
Mobility	150-200 cm^2/Vs
Resistivity	10^6 ΩV/cm
Bandgap	1,43 eV

There are three parameters for the geometry of the antenna, which are gap width w, gap distance g and length of the antenna that are illustrated in figure 2.2. The values of gap width w, gap distance g and length of the photoconductive antenna used were 10 μm, 6 μm and 44 μm respectively.

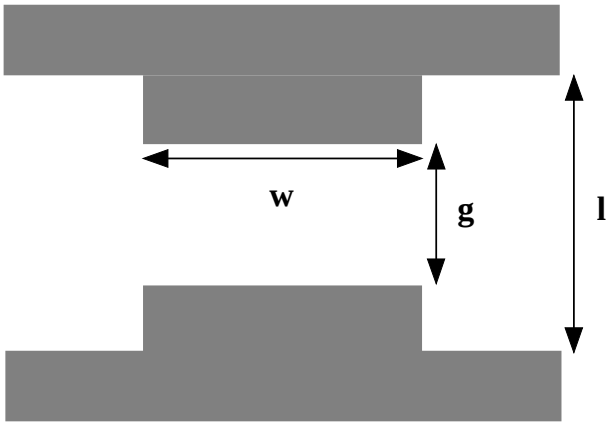

Figure 2.2: Geometrical structure of antenna

Among these parameters gap distance and length of the antenna are important parameters. The gap distance is important for laser excitation. On the other hand, the length determines the resonance condition for the frequency of emitted radiation. The resonance condition is defined by considering the antenna as a dipole of length, l. Terahertz resonance frequency of photoconductive antenna is given by

$$f = \frac{2cn}{l} \tag{2.1}$$

where
f is the terahertz resonance frequency,
c is the velocity of the light,
l is the length of the antenna.

The respective terahertz resonance frequency at 800 nm is 1 THz. The photographic front and back views of our photoconductive antenna is given in figure 2.3 and magnified image of its structure is shown in figure 2.4.

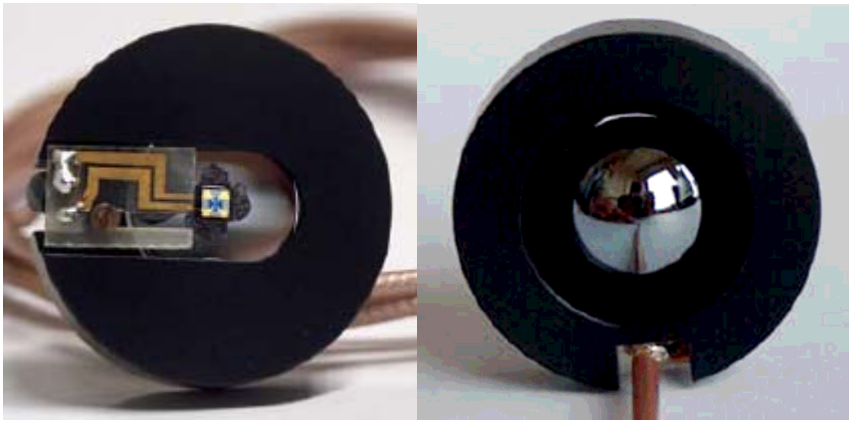

Figure 2.3: Front and back view of the photoconductive antenna [87].

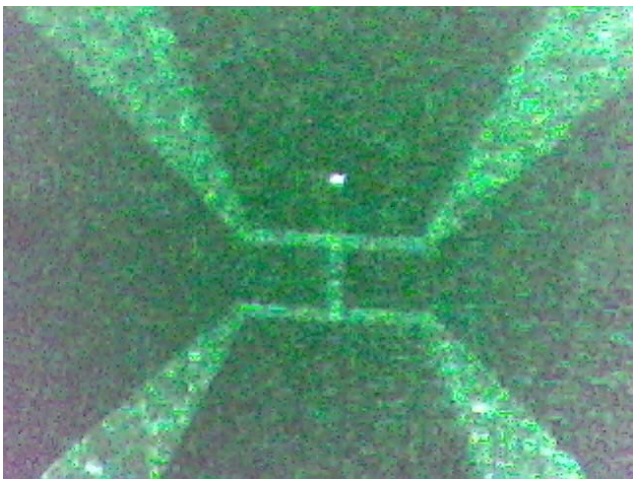

Figure 2.4: image of the antenna structure.

Terahertz radiation is obtained by applying bias voltage and phase modulation with a function generator. Bias voltage is needed for accelerating the free carriers in the antenna whereas phase modulation is necessary to read a signal from lock-in amplifier.

In order to collimate the terahertz radiation reflective optics were used. We used two Melles Griot 2.5" off-axis 90-degree parabolic mirrors with 11.68 cm focal length in our system. The first parabolic mirror collimated the emitted terahertz radiation and the second mirror focused it onto the detection crystal. Our detection crystal was <110> oriented ZnTe crystal with 1 mm thickness. Its refractive index at optical wavelength can be found through the relation [34]

$$n^2 = 4.27 + \frac{3.01\lambda^2}{\lambda^2 - 0.142} \tag{2.2}$$

In addition refractive index of ZnTe crystal at terahertz frequencies are given by the following formula [88],

$$n^2 = \frac{289.27 - 6\nu_{THz}^2}{29.16 - \nu_{THz}^2} \tag{2.3}$$

According to these formulas the refractive index of the crystal at 800 nm and 1 THz is 2.85 and 3.17 respectively.

In the detection arm, 1” corner cube mirror was used, which was mounted on Thorlabs DC-servo translation stage. By moving the corner cube time delay between the pump and probe beam was varied. After the corner cube laser light was directed on to the ZnTe crystal with a plane mirror. Next a plano-convex lens with 30 cm focal length was placed before the ZnTe crystal to better focus the probe beam on it. Subsequently quarter wave plate and Wollaston prism was placed behind the crystal successively.

Then the signal was detected by using a New Focus model 2307 large area balanced photodetector. Afterwards the signal was measured with phase sensitive detector called a lock-in amplifier. The lock-in amplifier we used in our system is SRS830

lock-in amplifier. Lock-in amplifier is a device that is capable of detecting signals as small as nanovolt even in presence of much higher noise. In fact it is a phase sensitive measurement. Thus it simultaneously detects both the magnitude and phase of a signal. According to Fourier's theorem input signal is represented by summation of sine functions having different amplitude, phase and frequency. Orthogonality of sinusoidal functions is basis of the working principle of the lock-in amplifier. One of these functions is input signal and the other is reference signal. Lock-in amplifier multiplies the input signal with the reference signal. When these two functions are equal to each other the lock-in amplifier integrates them over a specified time. In contrary to this if they are not equal, the detected signal is zero. With this working principle contribution from any other signal with different phase is prevented. Consequently a reference phase is required to perform a measurement with lock-in amplifier that is usually provided by either a function generator or chopper. Usually an input signal is followed with a noise, which is a variable function with different frequencies. However noise signals with different frequency than the reference signal is blocked by the lock-in amplifier. This is a significant advantage of the lock-in amplifier.

Finally with help of a labview control program the total distance and step size of movement of the translational stage was controlled through the THORLABS APT motor. Hence the data used for mapping out the terahertz waveform was taken with this labview control program.

2.3 SYSTEM OPERATION

At first hand Ti:Sapphire laser is mode-locked at 792 nm with 102 nm FWHM. The laser power was 341 mW after 4 W pump power. After the mode-locking process, construction of the spectrometer started with placing the beam splitter to split the laser light into two. Since the laser power for both the generation arm and detection arm was too high, two filters were put in both arms to attenuate the laser power. The power was decreased to 20 mW in generation arm and 8 mW in detection arm.

In addition to the power of laser, optical path lengths of both the generation and detection are another important parameter for the system. For electro-optic detection, probe beam and terahertz beam must be spatially and temporally coincident at the detection crystal. In this respect, optical path lengths of the two arms must be equal to each other to make the probe beam and terahertz beam arrive at the crystal simultaneously. To achieve this situation in our system, after the beam splitter four plane mirrors were put to obtain the necessary extra optical path in generation arm. After the plane mirrors, objective was placed. However for better alignment, before the objective was placed a pinhole was put and adjusted in such a way that it transmitted the maximum intensity of light. Next an objective was placed in front of the pinhole and again adjusted in a way that it transmitted the maximum intensity of light. Afterwards the photoconductive antenna was placed just behind the objective and subsequently the pump beam illuminated the antenna to generate the terahertz beam. Since the laser light was s-polarized, the photoconductive antenna was placed at a specific orientation allowing the laser light to pass through its gap with the correct direction. Next, alignment of the antenna was done by varying its position in three directions (x, y, z). Optimum position was decided by reading minimum resistance in the antenna, which was 353 kΩ in our system. In order to generate terahertz pulses, a function generator was used to apply peak-to-peak 10 V bias voltage to the antenna at a 2.5 kHz chopping frequency.

The generated terahertz beam was collimated and focused by the two parabolic mirrors. The mirrors were localized with help of another laser at visible wavelength, which was He-Ne laser with 17 mW power. At first, the laser was directed to the back side of the antenna to check whether the reflected light from the parabolic mirror was circular or not. Considering the shape of the reflected laser light, it was possible to understand whether the photoconductive antenna was at the focus of the parabolic mirror or not. If the antenna was at the focus then the reflected light must be circular in shape. On the contrary, if the reflected light had an elliptical shape it was obvious that the position of the mirror was wrong. In order to localize the first parabolic mirror, it was moved until the reflected light became circular. Then second parabolic mirror was put against the first parabolic mirror. To find the right position

of the second parabolic mirror, it was moved until all of the reflected light fell on it. After these adjustments both parabolic mirrors were moved in x-y-z directions to optimize their position. The focal length of both parabolic mirrors was 11.68 cm. But optimum distance between the photoconductive antenna and the first mirror was different. In order to find the optimum position of the first parabolic mirror we compared four measurements with different antenna-parabolic mirror distances. These values are given in table 2.5. According to the measurements, the obtained optimum position was 10.5 cm. On the other hand the optimum distance between the second parabolic mirror and ZnTe crystal was found to be 10,3 cm instead of the 11.68 cm focal length of the mirror.

Table 2.5: Antenna-mirror distance versus corresponding signal values

DISTANCE BETWEEN PARABOLLIC MIRROR AND ANTENNA	THz PULSE PEAK AMPLITUDE MEASURED BY LOCK-IN AMPLIFIER
12 cm	0,78 mV
11,8 cm	0,79 mV
11 cm	0,924 mV
10,5 cm	0,986 mV

In the detection arm, the laser was first directed to the corner cube fixed at a specific height, where after both incident and reflected beams were at the same height. The corner cube was mounted on a translational stage, which was connected to the APT motor. The time delay between the probe and pump beam was created by moving the corner cube back and forth. This movement of the motor and subsequently the corner cube was controlled with a labview program.

The frequency resolution achievable is determined by the total scanning length. The frequency resolution between two consecutive data points in the frequency spectrum

is given by

$$\Delta f = \frac{c}{2l} \tag{2.4}$$

where c is the speed of light and l is the total scanning length. Hence the separation in frequency domain with 1024 data points and 20 μm step size is 7.32 GHz. Afterwards the corner cube, a plane mirror was positioned to direct the probe beam onto the ZnTe crystal. Subsequently, a lens was placed in order to focus the probe beam onto the detection crystal. The focal length of the lens used was 30 cm but despite this its optimum position was 31 cm.

The incident terahertz beam induces a birefringence in ZnTe crystal causing a phase modulation in the propagating probe beam. To obtain more efficient electro-optic signal phase mismatch between probe and terahertz beam is an important parameter. In our system the phase mismatch was minimized by copropagating the terahertz and probe beams inside the detection crystal.

Finally, detection part of the spectrometer was constructed. Behind the ZnTe crystal quarter wave plate, Wollaston prism and photodetector was successively placed. In order to obtain the electro-optic signal terahertz pulse and probe pulse must be both temporally and spatially coincident at the electro-optic crystal. In addition, orientation of the crystal is influential on the detected signal. In order to obtain maximum electro-optic signal, angle between the polarization directions of the terahertz and probe beam must be either 0º or 90º [61]. In this respect optimum angle providing maximum signal was found by rotating the ZnTe crystal. In addition to the detection crystal, orientation of the quarter wave plate and Wollaston prism is also important. The Wollaston prism separates the probe beam into two orthogonolized linearly polarized light beams diverging from each other at an angle. In order to detect the electro-optic signal, a balanced photodetector was used to sense the intensity difference between these two beams. By rotating the Wollaston prism the two-separated light beams were made to fall on the two sensors of the photodetector.

Finally the photodetector was connected to lock-in amplifier to measure a signal that is proportional to the terahertz electric field. In this system, to obtain the reference signal necessary to make a measurement using the lock-in amplifier, we used a function generator that gave a square wave at 2.5 kHz.

2.4 SAMPLE MEASUREMENTS

Terahertz time domain spectroscopy is capable of unique spectroscopic measurements in the terahertz region. Hence it is a powerful tool for measurements at terahertz frequencies. In terahertz time domain spectroscopy, the measurements are based on the change of terahertz electric field between terahertz electric fields propagating through a sample and free space. As its name indicates data acquisition in terahertz time domain spectroscopy is made in time domain by recording the temporal shape of electric field strength of the terahertz pulse.

Since the measurement is based on a change in the obtained data with and without the sample, the measurement must be made for each case. The pulse propagating through the sample is called sample pulse whereas the pulse propagating through free space is called reference pulse. In this section some examples of this measurement are given. A typical measurement for terahertz pulse propagating through free space is demonstrated in figure 2.5.

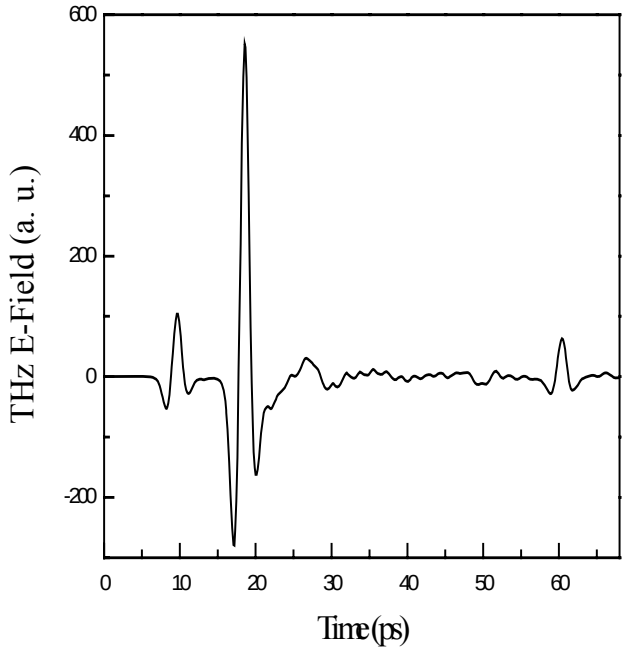

Figure 2.5: Terahertz waveform measured in free space

In time-domain terahertz spectroscopy, the measurements are made in the time domain. However, it is possible to obtain spectral components of both reference and sample pulses by applying Fourier transform to each measurement. In addition to spectral components phase information is also obtained from Fourier transformed data of the pulses. The complex electric field of terahertz pulse obtained through Fourier transform is given by

$$E(z,\omega) = \frac{1}{2\pi} \int_{-\infty}^{\infty} E(z,t) e^{-i\omega t} dt \tag{2.4}$$

where E(z, ω) is the complex electric field amplitude in frequency domain and E(z,t) is the experimentally measured electric field in time domain. In figure 2.6 Fourier transform of the terahertz pulse measured in time domain is illustrated.

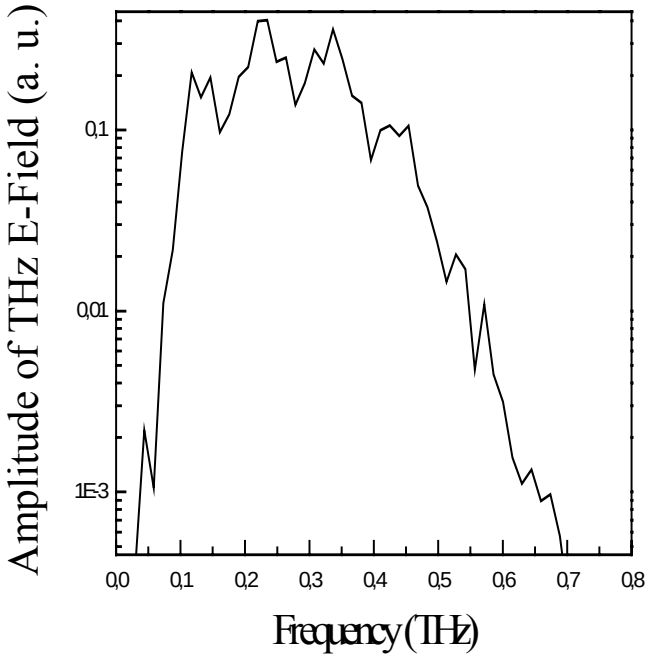

Figure 2.6: Amplitude of complex electric field of the terahertz pulse

As an example of measurement with terahertz time domain spectroscopy measurement of GaSe having 430 μm thickness and reference pulse is given in figure 2.7. In this figure the bigger main pulse is the reference terahertz pulse while that of the smaller is the sample pulse. Some distortions are present in both terahertz waveforms such as the minor pulses existing before and after the terahertz pulses. The prepulse infront of the main terahertz pulse is due to the gate reflection. On the other hand the small pulse following the main pulse is result of reflected terahertz pulse at the crystal-air interface. Because of this reflection, terahertz pulse is sampled for second time and this small pulse is observed. Several things can be observed by analyzing these terahertz waveforms. Firstly, sample pulse is weaker than the reference pulse. This indicates that only part of the incoming pulse is transmitted through the sample while the rest is either absorbed, reflected or scattered. Secondly, the sample pulse propagates later than the reference pulse. This is the result of the refractive index of the sample since it takes more time to

propagate through a medium compared to free space. In addition it shows the phase difference sensed by the terahertz pulse, which is a significant property of terahertz time domain spectroscopy.

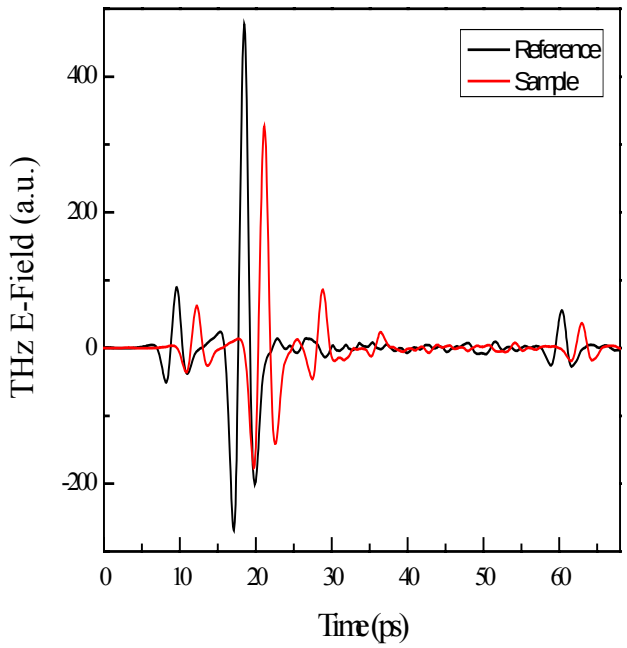

Figure 2.7: Mesurement of free space and GaSe crystal in time domain.

In order to extract properties of the material under study, Fourier transform must be applied to the data sets of both reference and sample pulses. The Fourier transformed data sets not only give amplitude but also phase of the complex electric field of the terahertz electric field. The Fourier transformed measurement of reference and sample pulse propagating through GaSe is shown in figure 2.8. In figure 2.8 only the amplitude of the spectral component is shown but phase information is calculated in Fourier transformation. According to the figure, amplitude spectrum of the sample pulse is weaker than the reference pulse similarly in time domain. The main reason for this is reflection and absorption of part of the terahertz pulse as it propagates through the GaSe crystal.

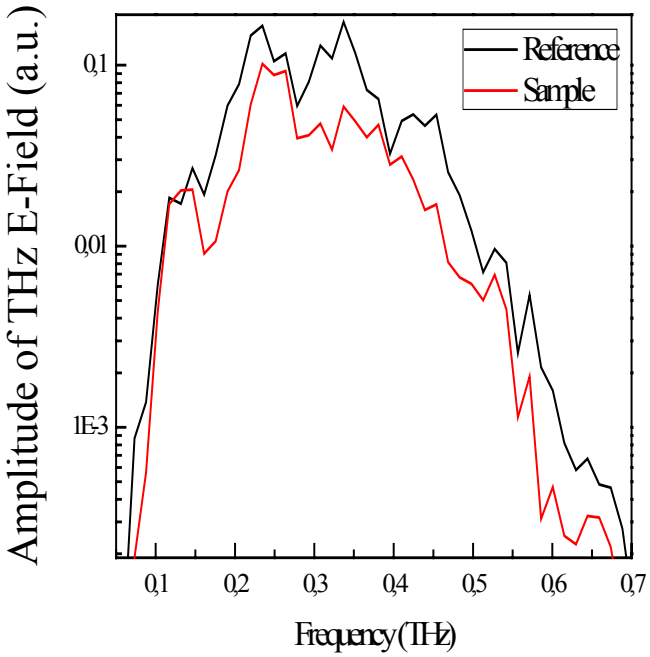

Figure 2.8: Spectra of reference and sample pulse.

In order to perform these measurements two TPX lenses are placed between the two parabollic mirrors and the sample is put at their focus as shown in figure 2.9. In our system we used TPX lenses having 50 mm diameter and 100 mm focal length. We calculate the radius and the confocal parameter of the focused terahertz beam by TPX lenses at 1 THz to be 0.366 mm and 2.806 mm respectively.

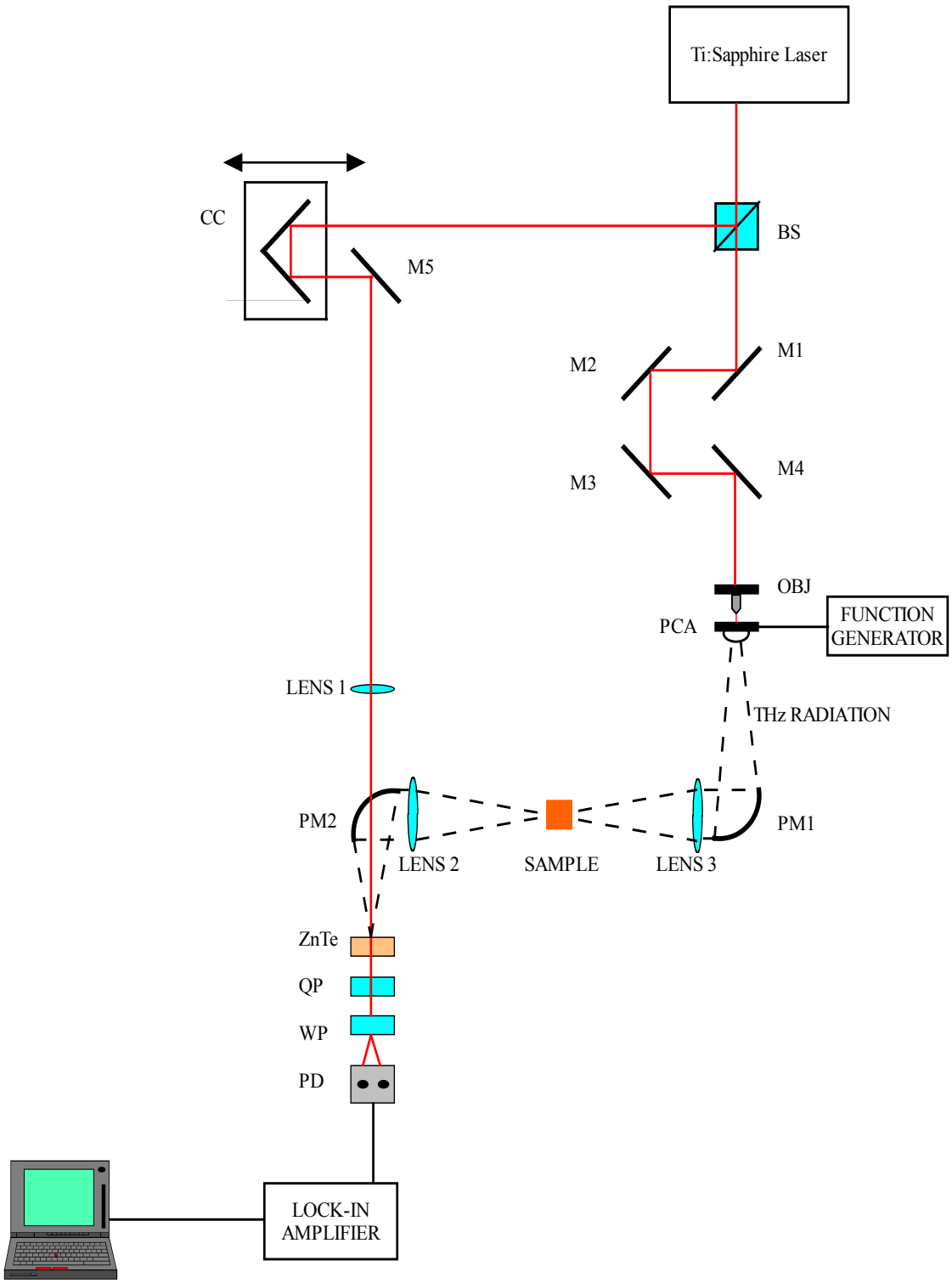

Figure 2.9: Illustration of the compact terahertz time domain spectrometer for sample measurement.

2.5 EXTRACTION OF SPECTROSCOPIC INFORMATION FROM THE THz-TDS RESULTS

In this section, we show how the spectroscopic information from experimental measurement is extracted and resulting information is described. In terahertz time domain spectroscopy refractive index of a material under study can be directly obtained. In fact refractive index consists of two components, which are real and imaginary parts. It can be represented as

$$\tilde{n}(\omega) = n_r(\omega) + in_i(\omega) \tag{2.5}$$

where n_r is real part and n_i is imaginary part of the refractive index. The wave vector contains complete information about the terahertz pulse and it is related to the complex refractive index $\tilde{n}(\omega)$ through the relation

$$k(\omega) = \frac{\nu\tilde{n}(\omega)}{c} \tag{2.6}$$

where ω frequency and c is is speed of light. The complex refractive index is also related to the permittivity through the relation

$$\varepsilon(\omega) = \tilde{n}(\omega)^2 \tag{2.7}$$

where $\varepsilon(\omega)$ is the permittivity. Furthermore, the imaginary part of the refractive index is related to the absorption coefficient by the equation

$$\alpha(\omega) = \frac{2\omega n_i(\omega)}{c} \tag{2.8}$$

where $\alpha(\omega)$ is the absorption coefficient.

In other types of spectroscopy, only intensity is measured but in terahertz time domain spectroscopy electric field is measured instead of intensity. Therefore it allows determination of not only the amplitude of electric field but also its phase information. The measurement is performed in time domain but it can be converted into frequency domain by Fourier transform. Hence the amplitude and phase information is obtained from the Fourier transform of the sample and reference pulse measurements. Electric field obtained from Fourier transform of the data is denoted as

$$E(\omega) = |E(\omega)| e^{i\varphi(\omega)} \tag{2.9}$$

where $E(\omega)$ is electric field vector, $|E(\omega)|$ is amplitude and $\varphi(\omega)$ is phase of the electric field. The power or magnitude of electric field and phase information of the Fourier transformed measured data is used for obtaining the real part of the refractive index and absorption coefficient of the material under study. The phase information is required for extracting the real part of the refractive index that is given by the formula

$$n_r = \frac{1}{kl}(\varphi(\omega, l) - \varphi(\omega)) \tag{2.10}$$

where l, k, $\varphi(\omega, l)$ and $\varphi(\omega)$ are the length of the sample, wave vector of the terahertz pulse, phase of the sample pulse and phase of the reference pulse respectively. This formula is valid for measurements performed in vacuum. However if the measurement is performed in air, its refractive index must be added to the calculated refractive index. In this case the refractive index formula (2.10) becomes

$$n_r = 1 + \frac{1}{kl}(\varphi(\omega, l) - \varphi(\omega)) \tag{2.11}$$

The imaginary part of the refractive index is obtained by using the ratios of the magnitudes of the electric fields of sample and reference pulse that is given by the relation

$$n_i = \frac{1}{kl}(\ln(\frac{E(\omega,l)}{E(\omega)})) \tag{2.12}$$

The imaginary part of the refractive index is related to the extinction coefficient. Therefore it is related to the absorbance through the formula (2.8). Hence the formula of absorption coefficient can be expressed more clearly as

$$\alpha(\omega) = \frac{\frac{2\omega}{kl}(\ln(\frac{E(\omega,l)}{E(\omega)}))}{c} \tag{2.13}$$

In these calculations any reflection or scattering at the sample interface that cause significant signal loss are not taken into account.

The refractive index and absorption coefficient of GaSe crystal in the frequency range 0.16 THz to 0.703 THZ are shown in figures 2.10 and 2.11 respectively. In the absorption graph, fringes are present due to the interference of the terahertz waves since in this range terahertz waves are much more longer than the thickness of the GaSe crystal.

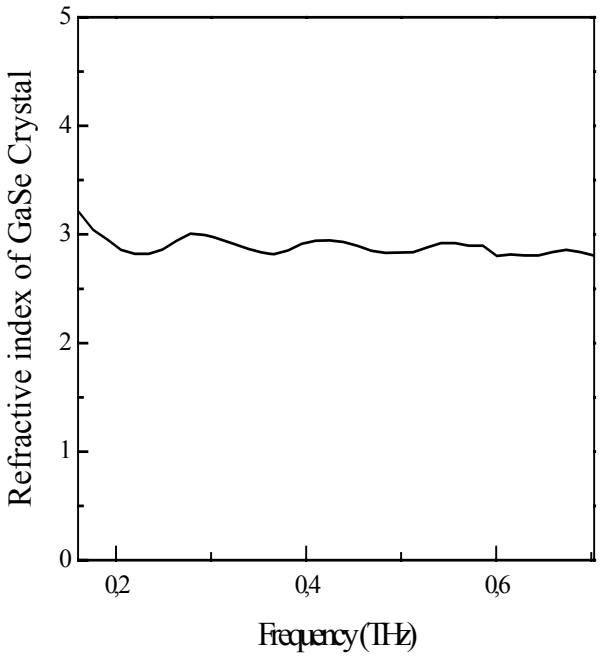

Figure 2.10: Refractive index of GaSe crystal at terahertz frequencies

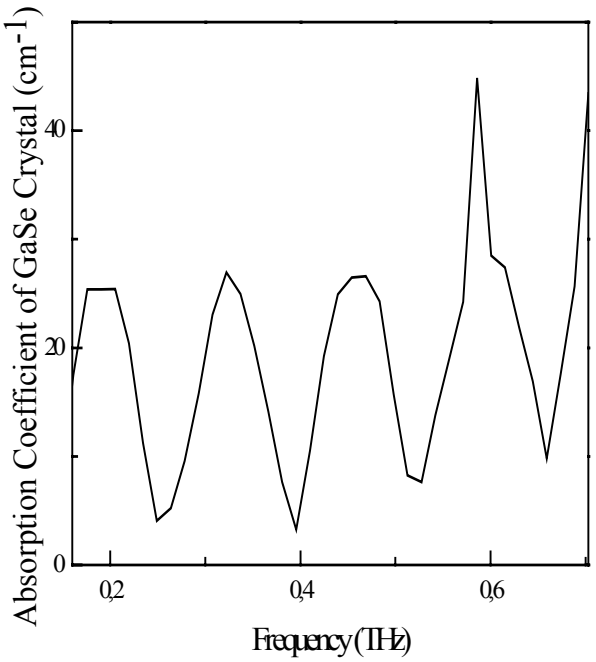

Figure 2.11: Absorption coefficient of GaSe crystal at terahertz frequencies

CHAPTER 3

POWER CHARACTERIZATION USING ELECTRO-OPTIC DETECTION

3.1 INTRODUCTION

It is possible to measure the power of terahertz radiation using bolometer. Its working principle is based on thermal detection of energy. Due to this reason bolometers are strongly affected by background thermal radiation unless they are cooled. To attain good detection sensitivity they need to be cooled with helium, which makes them bulky and expensive. Therefore they are not practical for terahertz power measurements. The other alternative is to simulate the power of the generated terahertz radiation. But when the THz pulse is generated with a photoconductive antenna it is difficult to exactly simulate the received power at the detector due to the efficiency of the transmitter and the THz collection optics. In this respect, it is necessary to introduce a new measurement technique of terahertz power by analyzing the received signal at the detector.

In this work, detection method used was electro-optic detection which is one of the basic and very popular detection methods for terahertz detection. Clearly there is a need for detailed information about this technique. Basic theory of electro optic detection was given in chapter one. In this chapter characterization of the detected

terahertz power using electro-optic detection is discussed.

In figure 3.1 terahertz waveform detected by using electro-optic detection is given. Distortions present in the waveform such as the minor pulses existing before and after the terahertz pulses and small oscillations following the main pulse have different origins. The prepulse infront of the main terahertz pulse is due to the gate reflection. On the other hand the small pulse following the main pulse is result of reflected terahertz pulse at the crystal-air interface interface. In fact because of this reflection, terahertz pulse is sampled for second time and this small pulse appears. In addition to the prepulse and the reflected pulse, there is also another distotion present in the measured terahertz waveform. It is clearly observed that some oscillations are present just behind the terahertz pulse. These oscillations are attributed to water vapour in air [62]. However, it is possible to avoid these oscillations by pumping nitrogen gas into the system.

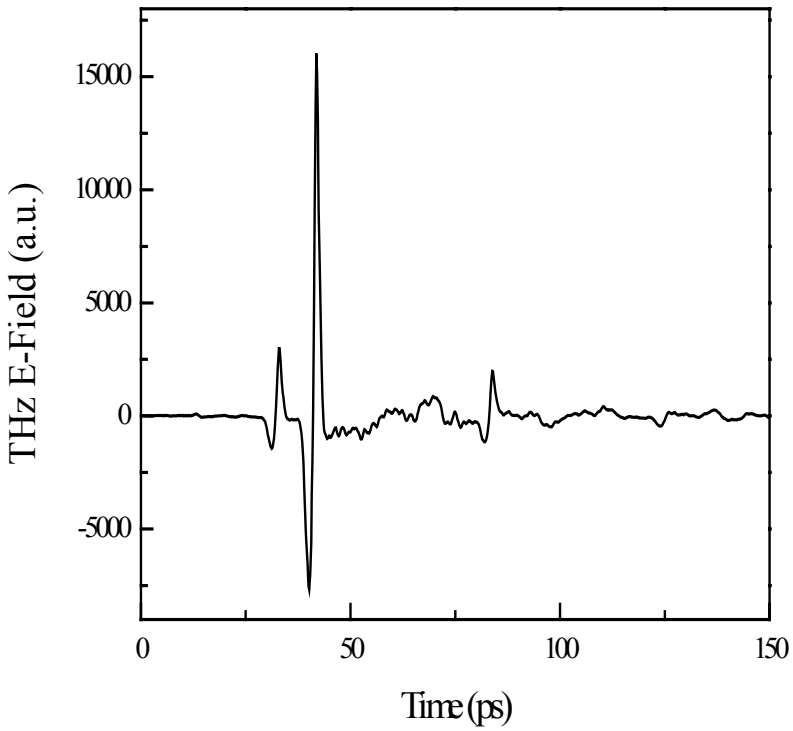

Figure 3.1: Terahertz waveform detected using electro-optic detection

3.2 POWER CHARACTERIZATION

In this section detected power of terahertz radiation using electro-optic detection is determined. However in calculations, power characterization is done at peak THz field. Therefore the power characterized is the peak power of the terahertz field. In order to find the average power further calculations are necessary.

Power characterization is given in three subsections. In the first part the birefringence induced in detection crystal by terahertz beam and the phase retardation experienced by probe beam are calculated. In the second part the measured electro-optic signal is analyzed. Finally, the two previous characterizations are combined to obtain a compact formula for the detected terahertz power.

3.2.1 CALCULATION OF BIREFRINGENCE DUE TO THz ELECTRIC FIELD

ZnTe crystal used for electro-optic detection is cubic and isotropic crsytal that is to say refractive index of crystal in all directions are equal to each other, with $\bar{4}3m$ symmetry group. In the presence of terahertz electric field birefringence is introduced in the crsytal and as a result of this refractive indices in different directions are no longer equal to each other. Hence the new equation for index ellipsoid following the procedures of [59],

$$\left(\frac{1}{n^2}\right)_1 x^2 + \left(\frac{1}{n^2}\right)_2 y^2 + \left(\frac{1}{n^2}\right)_3 z^2 + 2\left(\frac{1}{n^2}\right)_4 yz + 2\left(\frac{1}{n^2}\right)_5 xz + 2\left(\frac{1}{n^2}\right)_6 xy = 1 \tag{3.1}$$

In the absence of electric field, cross terms vanish and the equation reduces to the index of ellipsoid for an isotropic crystal,

$$\frac{x^2}{n_x^2}+\frac{y^2}{n_y^2}+\frac{z^2}{n_z^2}=1 \tag{3.2}$$

Change in refractive index in different directions of crystal due to applied terahertz electric field is related to both the electro-optic tensor and terahertz electric field in corresponding directions. The change is defined by

$$\Delta\left(\frac{1}{n^2}\right)_i=\sum_{j=1}^{3} r_{ij}E_j \tag{3.3}$$

where r_{ij} is electro-optic tensor.

The matrix form of equation (3.3) is expressed by,

$$\begin{pmatrix} \Delta\left(\frac{1}{n^2}\right)_1 \\ \Delta\left(\frac{1}{n^2}\right)_2 \\ \Delta\left(\frac{1}{n^2}\right)_3 \\ \Delta\left(\frac{1}{n^2}\right)_4 \\ \Delta\left(\frac{1}{n^2}\right)_5 \\ \Delta\left(\frac{1}{n^2}\right)_6 \end{pmatrix} = \begin{pmatrix} r_{11} & r_{12} & r_{13} \\ r_{21} & r_{22} & r_{23} \\ r_{31} & r_{32} & r_{33} \\ r_{41} & r_{42} & r_{43} \\ r_{51} & r_{52} & r_{53} \\ r_{61} & r_{62} & r_{63} \end{pmatrix} \times \begin{pmatrix} E_{THz_x} \\ E_{THz_y} \\ E_{THz_z} \end{pmatrix} \tag{3.4}$$

The form of electro-optic tensor depends on the internal symmetry of the material. For ZnTe crystal electro-optic tensors except three terms are zero and these three tensors are equal to each other. That is

$$r_{41} = r_{52} = r_{63} \tag{3.5}$$

Then the equation for index ellipsoid for ZnTe crystal becomes

$$\frac{x^2}{n^2} + \frac{y^2}{n^2} + \frac{z^2}{n^2} + 2r_{41}^{yz} E_{THz_x} + 2r_{41}^{xz} E_{THz_y} + 2r_{41}^{xy} E_{THz_z} = 1 \tag{3.6}$$

In the absence of electric field (x, y, z) were the principal axes of crystal. However in the presence of terahertz electric field cross terms are present. In order to get rid of the cross terms in the equation (3.6) coordinate transformation is done and subsequently new axes are introduced as principal axes. But these axes are no longer coincident with the original principal axes. If the direction of applied electric field is chosen to be z-direction, the equation (3.6) becomes

$$\frac{x^2}{n^2}+\frac{y^2}{n^2}+\frac{z^2}{n^2}+2r_{41}xyE_{THz}=1 \tag{3.7}$$

However there is still a cross term in the equation. In order to get rid of the cross term this equation must be put in the form of equation (3.8), which is equation of index ellipsoid for isotropic crystal such that

$$\frac{x'^2}{n^2}+\frac{y'^2}{n^2}+\frac{z'^2}{n^2}=1 \tag{3.8}$$

The necessary coordinate transformation is achieved if the original coordinate system is rotated by 45º around z-axis. Another way is to diagonalize the matrix by finding the corresponding eigenvalues. With using the former way the equation (3.7) is transformed in to equation (3.8). The rotation of the axes and new coordinate system is shown in figure 3.2.

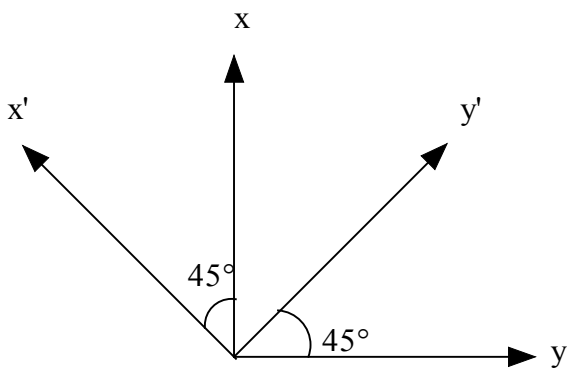

Figure 3.2: Transformation of axes

The transformation matrix is given by

$$\begin{bmatrix} x' \\ y' \\ z' \end{bmatrix} = \begin{bmatrix} \frac{1}{\sqrt{2}} & \frac{1}{\sqrt{2}} & 0 \\ -\frac{1}{\sqrt{2}} & \frac{1}{\sqrt{2}} & 0 \\ 0 & 0 & 1 \end{bmatrix} \times \begin{bmatrix} x \\ y \\ z \end{bmatrix} \tag{3.9}$$

Old axes in terms of transformed coordinates are expressed as

$$x = x'\cos 45 - y'\sin 45 \tag{3.10}$$

$$y = y'\cos 45 + x'\sin 45 \tag{3.11}$$

$$z = z' \tag{3.12}$$

By using these equations new coordinates are obtained as

$$x' = \frac{x + y}{\sqrt{2}} \tag{3.13}$$

$$y' = \frac{y - x}{\sqrt{2}} \tag{3.14}$$

$$z' = z \tag{3.15}$$

So the equation (3.7) is put in the form

$$\frac{1}{2n^2}\left(x'^2 + y'^2 - 2x'y'\right) + \frac{1}{2n^2}\left(x'^2 + y'^2 + 2x'y'\right) + \frac{z'^2}{n^2} + r_{41}\left(x'^2 - y'^2\right)E_{THz} = 1 \tag{3.16}$$

By collecting the x', y' and z' terms the equation becomes

$$\left(\frac{1}{n^2} + r_{41}E_{THz}\right)x' + \left(\frac{1}{n^2} - r_{41}E_{THz}\right)y' + \frac{z'^2}{n_z'^2} = 1 \tag{3.17}$$

where $$\frac{1}{n_x'^2} = \frac{1}{n^2} + r_{41}E_{THz} \tag{3.18}$$

and $$\frac{1}{n_y'^2} = \frac{1}{n^2} - r_{41}E_{THz} \tag{3.19}$$

By using the approximation $\frac{1}{n^2} \gg r_{41}E_{THz}$, the term $r_{41}E_{THz}$ is treated as perturbation in equation (3.17). After taking the derivative of term $\frac{1}{n^2}$, it becomes

$$\Delta\left(\frac{1}{n^2}\right) = -\frac{2}{n^3}\Delta n \tag{3.20}$$

This gives Δn as

$$\Delta n = -\frac{1}{2} n^3 \Delta\left(\frac{1}{n^2}\right) \tag{3.21}$$

As a result of this approximation refractive indices along the new axes become

$$n_x^{'} = n_x - \frac{1}{2} {n_x}^3 \Delta\left(\frac{1}{{n_x}^2}\right) \tag{3.22}$$

$$n_y^{'} = n_y + \frac{1}{2} {n_y}^3 \Delta\left(\frac{1}{{n_y}^2}\right) \tag{3.23}$$

$$n_z^{'} = n_z \tag{3.24}$$

The refractive indices in old x-y and z-directions are equal to ordinary refractive index n_o and extraordinary refractive index n_e respectively. Consequently, refractive indices in new principal axis directions are given as

$$n_x^{'} = n_O - \frac{1}{2} {n_O}^3 r_{41} E_{THz} \tag{3.25}$$

$$n_y^{'} = n_O + \frac{1}{2} {n_O}^3 r_{41} E_{THz} \tag{3.26}$$

$$n_Z^{'} = n_e \tag{3.27}$$

Since the birefringence is defined as the refractive index difference in x and y directions, it is given by,

$$n_y' - n_x' = n_o^3 r_{41} E_{THz} \tag{3.28}$$

Due to the birefringence, optical pulse propagating through ZnTe crystal is subjected to phase retardation. Its x and y components will propagate with different velocities inside the crystal. The phase difference between these two components is expressed as

$$\Gamma = \frac{\omega}{c}\left(n_y' - n_x'\right)L \tag{3.29}$$

where Γ is phase retardation and L is the crystal thickness. After substituting the birefringence into the formula (3.29) phase retardation becomes

$$\Gamma = \frac{2\pi}{\lambda} n_o^3 r_{41} L E_{THz} \tag{3.30}$$

3.2.2 CALCULATION OF SIGNAL

In this section, calculation for electro-optic signal is given. In these calculations, refractive indices and induced polarization directions of probe beam are assumed to be known as in [89]. In electro-optic detection setup probe beam first propagates through ZnTe crystal, and then it propagates through quarter wave plate and Wollaston prism as shown in figure 3.3.

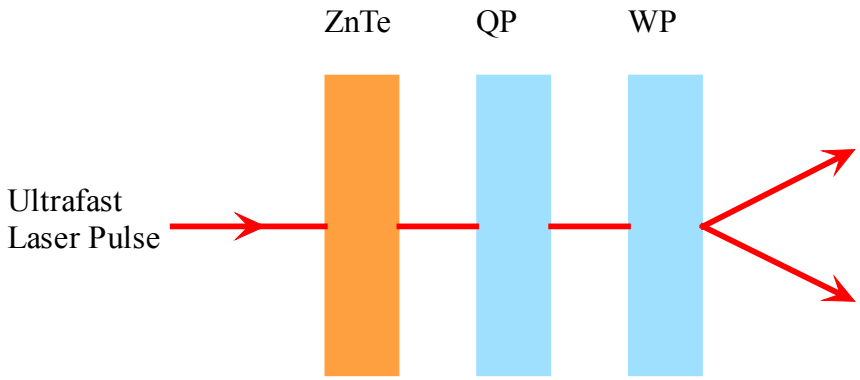

Figure 3.3: Electro-optic detection setup

As the probe beam propagates through the ZnTe crystal its two modes experience a phase difference due to the induced birefringence from the terahertz beam. Because of this phase difference previously linearly polarized probe beam becomes elliptically polarized. The ZnTe crystal is followed by quarter wave plate and Wollaston prism. In consequence the initial polarization directions of the two modes of the probe beam change as the probe beam propagates through these three optical elements. The relative orientation of initial and final polarization directions of two modes of probe beam after the quarter wave plate and Wollaston prism are illustrated in figure 3.4.

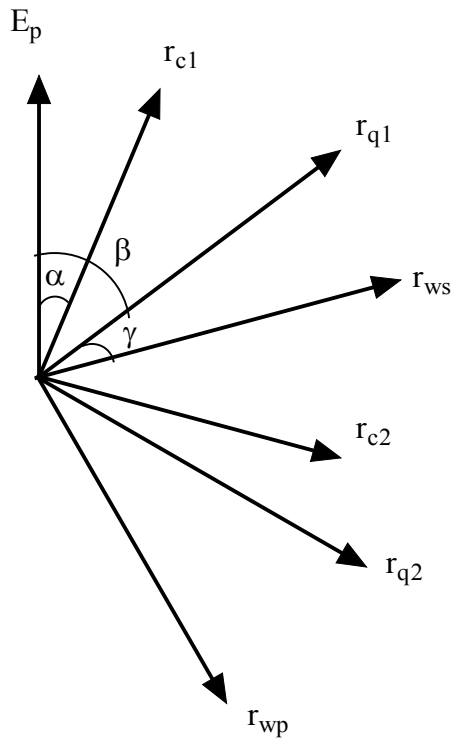

Figure 3.4: The relative orientation of initial polarization direction of probe beam, two modes in the crystal and quarter wave plate.

In this geometry,

$\hat{E}_p$ is unit vector corresponding to the initial polarization direction of probe beam,

$\hat{r}_{c_1}$ and $\hat{r}_{c_2}$ are unit vectors corresponding to polarization directions of the probe beam propagating through the crystal,

$\hat{r}_{q_1}$ and $\hat{r}_{q_2}$ are unit vectors corresponding to polarization directions of the probe beam propagating through the quarter wave plate,

$\hat{r}_{w_s}$ and $\hat{r}_{w_p}$ are the s-polarized and p-polarized components of the probe beam that the Wollaston prism splits

The unit vector indicating the initial polarization direction of probe beam can be expressed in terms of directions of two propagation modes in ZnTe crystal that is given by,

$$\hat{E}_p = \left(\hat{r}_{c_1} \bullet \hat{E}_p\right)\hat{r}_{c_1} + \left(\hat{r}_{c_2} \bullet \hat{E}_p\right)\hat{r}_{c_2} \tag{3.31}$$

After propagating through the crystal, each propagation mode will experience a phase difference proportional to the corresponding refractive index of each mode. So after the crystal the initial unit vector of the probe beam becomes

$$\hat{E}_{pc} = e^{\frac{i\omega n_1 L}{c}}\left(\hat{r}_{c_1} \bullet \hat{E}_p\right)\hat{r}_{c_1} + e^{\frac{i\omega n_2 L}{c}}\left(\hat{r}_{c_2} \bullet \hat{E}_p\right)\hat{r}_{c_2} \tag{3.32}$$

where

$\hat{E}_{pc}$ is unit vector showing the polarization direction of probe beam after the crystal,

ω is the frequency of probe beam,

L is the crystal thickness,

n_1 and n_2 are the refractive indices of two propagation modes of the crystal,

c is the speed of light.

By using the geometry shown in figure 3.4 the dot product terms in equation (3.32) are equal to

$$\hat{r}_{c_1} \bullet \hat{E}_p = \cos\alpha \tag{3.33}$$

$$\hat{r}_{c_2} \bullet \hat{E}_p = \cos\left(90 + \alpha\right) = -\sin\alpha \tag{3.34}$$

After substituting these into the formula (3.32) the unit vector indicating polarization direction of probe beam becomes,

$$\hat{E}_{pc} = e^{\frac{i\omega n_1 L}{c}} \cos\alpha \hat{r}_{c_1} + e^{\frac{i\omega n_2 L}{c}} (-\sin\alpha)\hat{r}_{c_2} = e^{\frac{i\omega n_1 L}{c}} \left[\cos\alpha \hat{r}_{c_1} - e^{\frac{i\omega \Delta n L}{c}} \sin\alpha \hat{r}_{c_2} \right] \tag{3.35}$$

By using approximation $\frac{\omega \Delta n L}{c} \ll 1$, I get $e^{\frac{i\omega \Delta n L}{c}} \approx 1 + \frac{i\omega \Delta n L}{c}$. Hence the equation can be approximated as

$$\hat{E}_{pc} \cong e^{\frac{i\omega n_1 L}{c}} \left[\cos\alpha \hat{r}_{c_1} - \left(1 + \frac{i\omega \Delta n L}{c}\right) \sin\alpha \hat{r}_{c_2} \right] \tag{3.36}$$

The equation is put in more simple form by letting $\zeta = \frac{\omega \Delta n L}{c}$. Then

$$\hat{E}_{pc} \cong e^{\frac{i\omega n_1 L}{c}} \left[\cos\alpha \hat{r}_{c_1} - (1 + i\zeta) \sin\alpha \hat{r}_{c_2} \right] \tag{3.37}$$

The same procedure is followed to consider the effect of the quarter wave plate on the polarization of the probe beam. After the probe beam passes through quarter wave plate, two propagating modes will experience 90º phase difference. The polarization of probe beam can be decomposed into two propagation modes of the quarter wave plate by introducing the complex phase factor as

$$\hat{E}_{pq} = \left(\hat{r}_{q_1} \bullet \hat{E}_{pc} \right) \hat{r}_{q_1} + i \left(\hat{r}_{q_2} \bullet \hat{E}_{pc} \right) \hat{r}_{q_2} \tag{3.38}$$

The imaginary term i is added to the formula to account for the 90º phase retardation. After evaluating the dot product terms equation becomes,

$$\hat{E}_{pq} \cong e^{\frac{i\omega n_1 L}{c}}\left[\cos(\beta-\alpha)\cos\alpha\hat{r}_{q_1} - (1+i\zeta)\sin\alpha\sin(\beta-\alpha)\hat{r}_{q_1}\right] + ie^{\frac{i\omega n_1 L}{c}}\left[-\sin(\beta-\alpha)\cos\alpha\hat{r}_{q_2} - (1+i\zeta)\sin\alpha\cos(\beta-\alpha)\hat{r}_{q_2}\right] \quad (3.39)$$

After collecting the common terms the equation simplifies to the following form,

$$\hat{E}_{pq} \cong e^{\frac{i\omega n_1 L}{c}}\left\{\left[\cos(\beta) - i\zeta\sin(\beta-\alpha)\sin\alpha\right]\hat{r}_{q_1} + \left[\zeta\sin\alpha\cos(\beta-\alpha) - i\sin\beta\right]\hat{r}_{q_2}\right\} \quad (3.40)$$

Finally the same method is applied for the Wollaston prism. The last polarization direction of probe beam can be written in terms of directions the two propagation modes in Wollaston prism in a similar way as

$$\hat{E}_{pw} = \left(\hat{r}_{w_1} \bullet \hat{E}_{pq}\right)\hat{r}_{w_1} + \left(\hat{r}_{w_2} \bullet \hat{E}_{pq}\right)\hat{r}_{w_2} \quad (3.41)$$

In Wollaston prism, probe beam is splitted into two linearly and orthogonally polarized beams. In consequence, the two components in equation (3.37) are treated separately. After the measurement of electro-optic signal is performed by measuring the intensity difference of these two beams. Since the two components of the previous equation can be calculated individually, the intensity of the each separated beam falling on the photodetector can be calculated. The total intensity of the beams are denoted as

$$I = \frac{1}{2}cn\varepsilon_0 |E|^2 \quad (3.42)$$

Continuing with this equation intensities of the two out coming beams are expressed as

$$I_1 = \frac{1}{2} cn\varepsilon_0 \left| \hat{E}_{pw} \bullet \hat{r}_{w_S} \right|^2 \tag{3.43}$$

$$I_2 = \frac{1}{2} cn\varepsilon_0 \left| \hat{E}_{pw} \bullet \hat{r}_{w_P} \right|^2 \tag{3.44}$$

Intensity of the first term is calculated as

$$I_1 \simeq I_{tot} \left[\left(\cos\beta - i\zeta \sin\left(\beta - \alpha\right) \sin\alpha \right) \cos\gamma + \left(\zeta \sin\alpha \cos\left(\beta - \alpha\right) - i \sin\beta \right) \sin\gamma \right]^2 \tag{3.45}$$

After expanding and simplifying the equation it becomes

$$I_1 \simeq I_{tot} \left[\cos^2\beta \cos^2\gamma + \sin^2\beta \sin^2\gamma + \frac{\zeta}{2} \sin\left(2\alpha\right) \sin\left(2\gamma\right) \right] \tag{3.46}$$

Similarly intensity of the second beam is given by,

$$I_2 \simeq I_{tot} \left[\cos^2\beta \sin^2\gamma + \sin^2\beta \cos^2\gamma - \frac{\zeta}{2} \sin\left(2\alpha\right) \sin\left(2\gamma\right) \right] \tag{3.47}$$

Hence the intensity difference between two beam are calculated as

$$\Delta I = I_1 - I_2 \simeq I_{tot} \left[\cos\left(2\beta\right) \cos\left(2\gamma\right) + \zeta \sin(2\gamma) \sin\left(2\alpha\right) \right] \tag{3.48}$$

According to this equation effect of the orientation of the Wollaston prism is given by the terms $\cos\left(2\gamma\right)$ and $\sin(2\gamma)$. This indicates that rotating the Wollaston prism

until the $\cos(2\gamma)$ term becomes zero can maximize the electro-optic signal detection sensitivity. In this case, the angle between the initial polarization direction of probe beam and quarter wave plate becomes irrelevant. This obliviously shows that if the orientation of the Wollaston prism with respect to quarter wave plate is right, then the orientation of both quarter wave plate and Wollaston prism with respect to the initial probe polarization is right too.

Moreover, maximizing the detection sensitivity also maximizes the obtained electro-optic signal. Therefore after maximizing the signal the intensity difference becomes

$$\Delta I \simeq I_{tot}\zeta \sin(2\gamma) \tag{3.49}$$

The intensities of each beam can be individually measured to find out both their sum and difference. In fact, what is measured in electro-optic detection is

$$\frac{\Delta I}{I_{tot}} \simeq \zeta \sin(2\gamma) \tag{3.50}$$

This expression points that changing the orientation of detection crystal enables further maximization of the electro-optic signal. Rotation of ZnTe crystal is performed in such a way that the term $\sin(2\gamma)$ is equal to its maximum value one. In case the electro-optic detection setup is aligned to have most efficient configuration, the signal obtained is maximum. Then the expression for the measured signal is

$$\frac{\Delta I}{I_{tot}} \approx \zeta = \frac{\omega \Delta n L}{c} \tag{3.51}$$

In consequence, the detected signal is linearly proportional to the refractive index difference in two propagation modes of the detection crystal and subsequently terahertz electric field. In addition polarization direction of probe beam is also an important parameter for the detected electro-optic signal. If the polarization direction

of the probe beam is parallel to the polarization direction of any modes of the detection crystal, the obtained electro-optic signal is zero. On the contrary, if they are perpendicular to each other the obtained signal is the topmost.

3.2.3 CALCULATION OF DETECTED POWER

In two previous subsections electro-optic signal and terahertz induced birefringence were calculated. To calculate the detected terahertz power they will be combined to have a simple expression. By substituting the calculated birefringence into the electro-optic signal formula the following expression is obtained:

$$\frac{\Delta I}{I_{tot}} = \frac{2\pi}{\lambda} n_o{}^3 r_{41} L E_{THz} \tag{3.52}$$

In this formula electro-optic signal is expressed as ratio of intensity difference and total intensity. However it can also be expressed in terms of power of each probe beam. Then the equation becomes

$$\frac{\Delta P}{P_{tot}} = \frac{2\pi}{\lambda} n_o{}^3 r_{41} L E_{THz} \tag{3.53}$$

Considering the formula above electric field of terahertz beam is obtained in straightforward way. For our system other parameters are as follows:

$r_{41} = 3.9 \times 10^{-12}$ m/V

$n_0 = 2.85$ (for λ=800 nm)

$\lambda = 800\,\text{nm}$

$L = 1$ mm

$\varepsilon_0 = 8.85 \times 10^{-12}$ C^2/Nm^2

Signal measured = $\frac{\Delta P}{P} = 3.12 \times 10^{-3}$

Terahertz pulse width = 1.46667 ps

Radius of terahertz beam = 0.346 mm

Repetition rate of laser = 70 MHz

The signal was obtained by measuring the intensity of each optic beam with using an optical power meter. After substituting these values in formula (3.49), it gives terahertz electric field as 44 V/cm. Since power is given as intensity times area in order to find out the power of terahertz beam its intensity must be known. Since its electric field is determined, intensity of terahertz beam is found through the following relation:

$$I = \frac{1}{2} cn\varepsilon_0 \left| E_{THz} \right|^2 \tag{3.54}$$

Putting the corresponding values into the formula above terahertz intensity is found and then multiplied by the area of terahertz beam. In these calculations radius of the terahertz beam was obtained by calculating its waist size at the detection crystal. Firstly, the exit diameter of the terahertz beam by the parabolic mirror is calculated with using the following formula,

$$d_{out} = f\theta = f \times \frac{1.22\lambda}{d_{in}} = 6.92 \times 10^{-4} m \tag{3.55}$$

In this formula focal length and entrance diameter of the terahertz beam was the focal length and diameter of the parabolic mirror. On the other hand, the wavelength was the wavelength of the terahertz beam at 1 THz, which is 300 μm. Since half of the exit diameter of the THz beam after the parabolic mirror is equal to its waist size, radius of THz beam on the detection crystal was calculated as 0.346 mm. Next area of the terahertz beam was calculated and multiplied by its intensity to obtain its power. As a result of this calculation gives peak power of terahertz beam was

calculated as 27.66 mW. The peak power is converted to average power by multiplying it with repetition rate of laser and pulse width of terahertz pulse. As a result of this multiplication average power was found to be 2.84 μW.

In previous works terahertz power was either measured using a bolometer or calculated using the obtained signal. For measurements with bolometer power of terahertz radiated from photoconductive antennas was found to be at the order of microwatts [90]. Furthermore, in another work terahertz power measured with using electro-optic signal was few microwatts [63, 91]. According to the calculations in this thesis the detected average terahertz power was also at the order of microwatts. This obviously shows that the characterized detected power is consistent with previous literature measurements.

3.3 INFLUENCE OF THE SPOT SIZE OF THE PROBE BEAM ON THE DETECTED THz POWER

In this section effect of spot size of probe beam on the detected terahertz power was analyzed. To explore this effect detected THz power for different probe beam spot sizes were compared. The spot size of the probe beam was changed with replacing the lens used in the system with lenses having different focal lengths. Moreover, in order to study further the relationship between detected terahertz power and spot size of the probe beam, effect of confocal parameters of probe beam on terahertz intensity profile was theoritically analyzed. The experimental and theoretical analysis are given in two subsections.

3.3.1 EXPERIMENTAL RESULTS

Power measurements were performed with lenses of focal length 20, 30 and 40 cm that is shown in the setup in figure 3.5. The respective terahertz waveforms in time

domain and frequency domain obtained with these lenses are shown in the figures 3.6, 3.7, 3.8, 3.9, 3.10 and 3.11 respectively. In each case similar terahertz waveform and power spectrums were obtained. But on the other hand, a change was observed in the measured signal $\frac{\Delta P}{P}$ for each of the three lenses which are shown in figures 3.12 and 3.13. Therefore, detected terahertz power in all three cases were different. The average terahertz power calculated with previously described method was 2.84 μW, 1.79 μW and 1.18 μW using lenses having 20 cm, 30 cm and 40 cm focal lengths respectively. The measurements indicate that as the spot size of the probe beam decreases, THz power increases linearly.

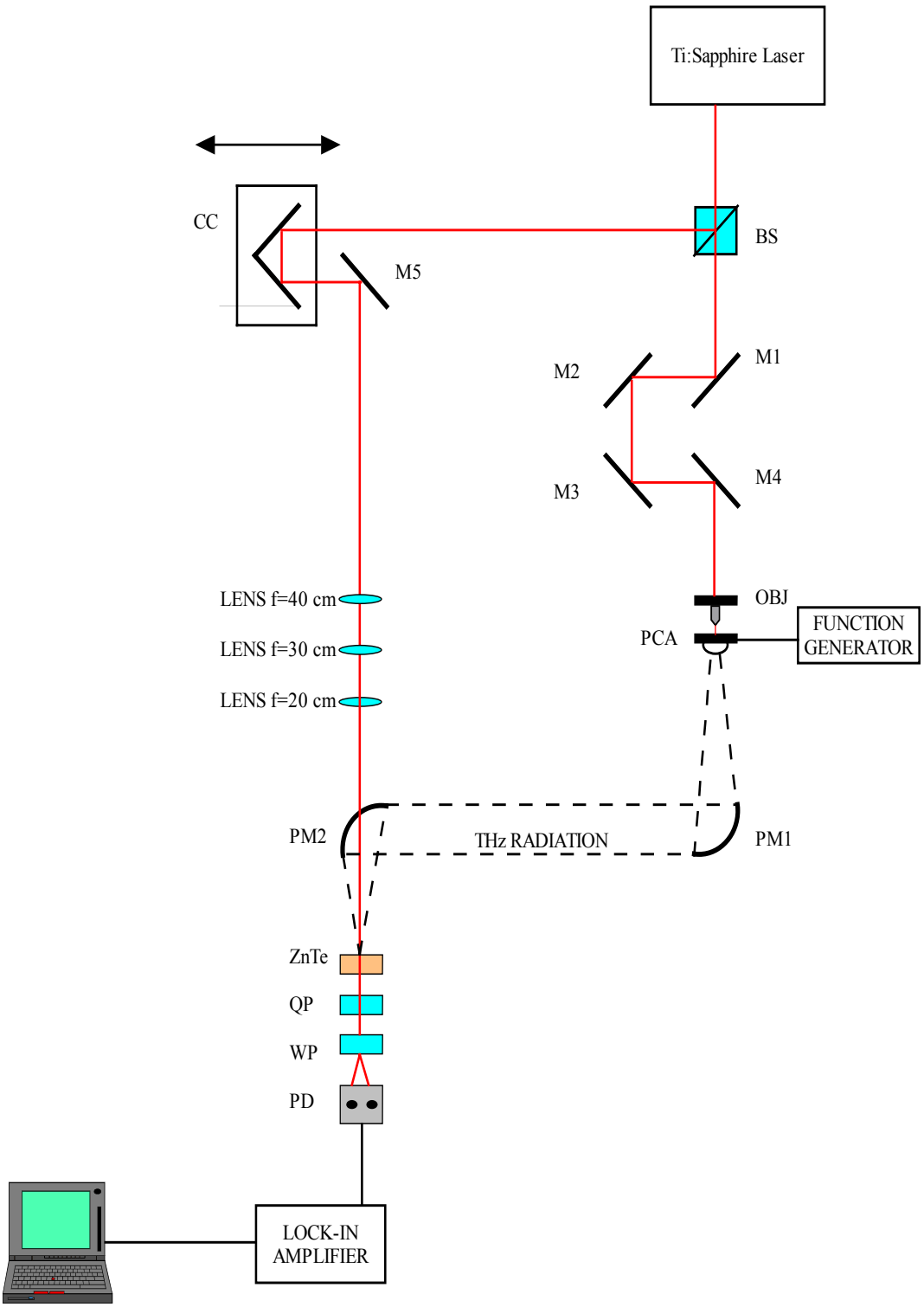

Figure 3.5: Schematic view of the terahertz time-domin spectrometer

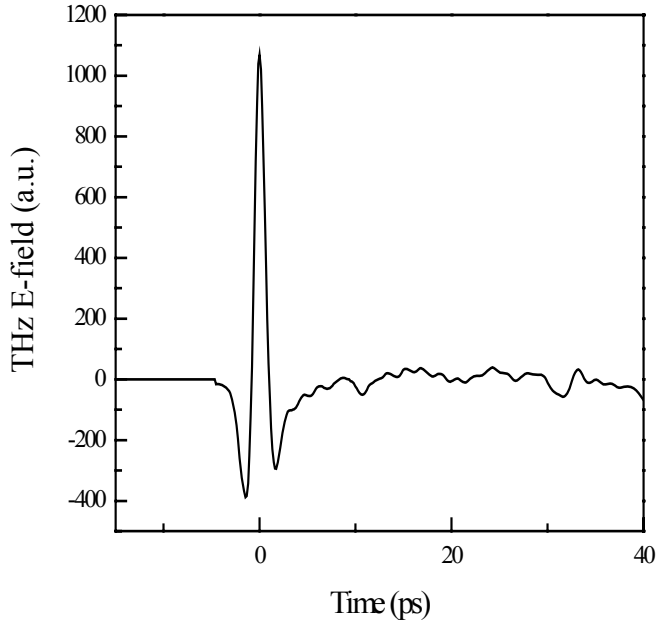

Figure 3.6: Terahertz waveform obtained by using a lens having 20 cm focal length.

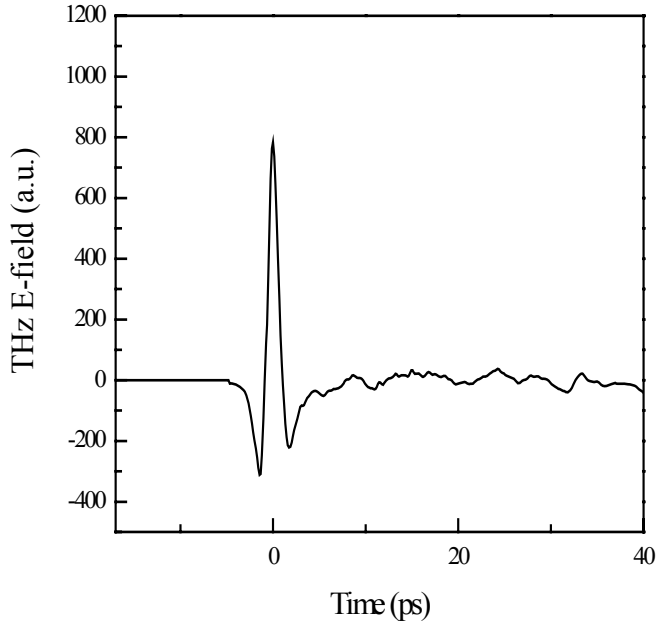

Figure 3.7: Terahertz waveform obtained by using a lens having 30 cm focal length.

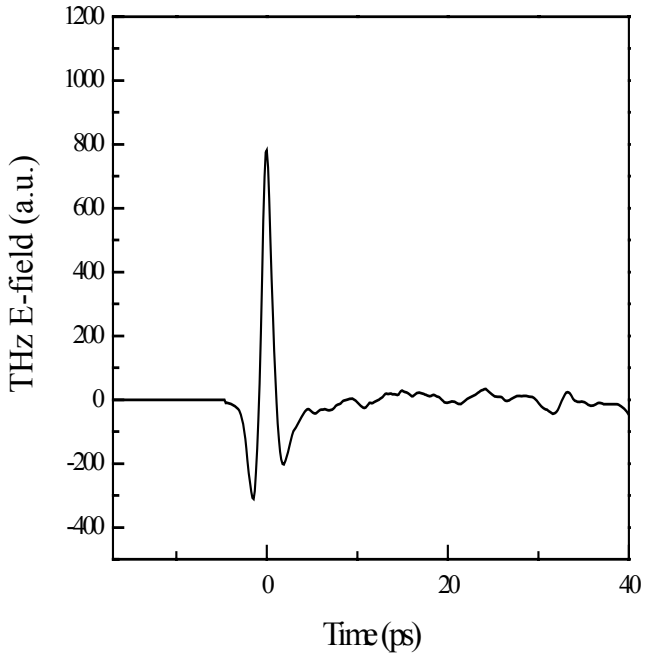

Figure 3.8: Terahertz waveform obtained by using a lens having 40 cm focal length.

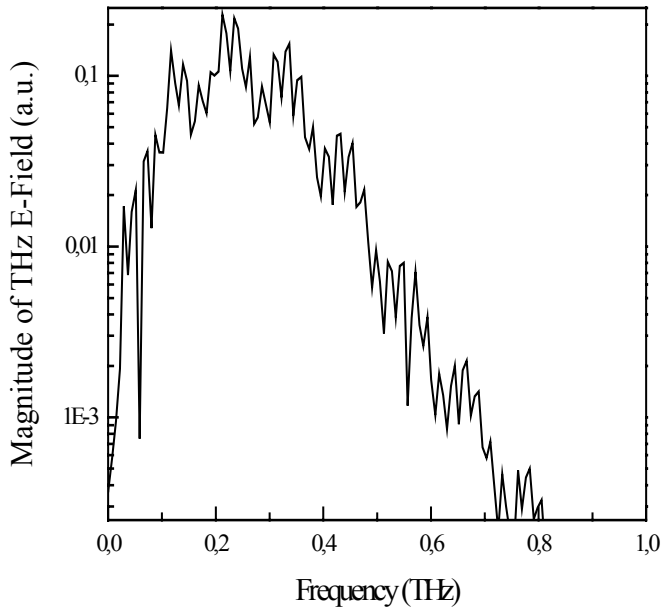

Figure 3.9: Magnitude of terahertz electric field obtained by using a lens having 20 cm focal length.

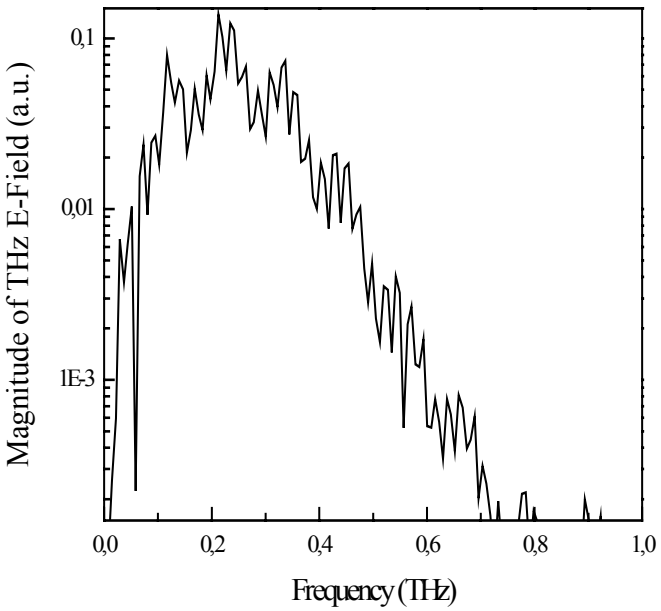

Figure 3.10: Magnitude of terahertz electric field obtained by using a lens having 30 cm focal length.

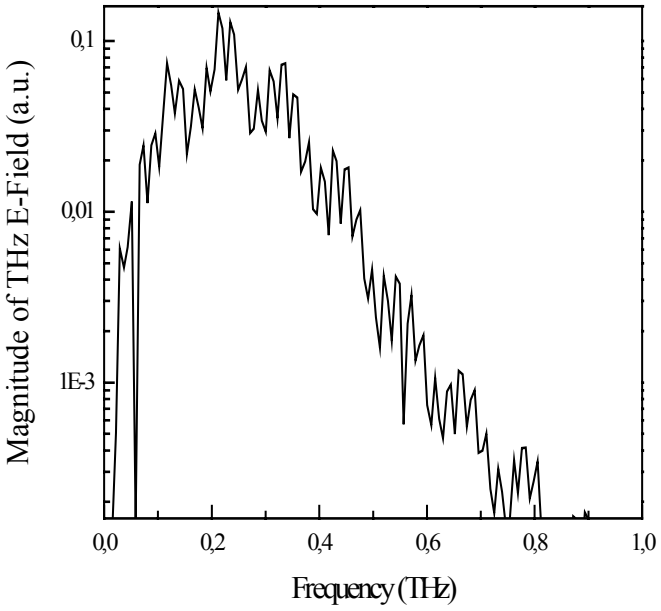

Figure 3.11: Magnitude of terahertz electric field obtained by using a lens having 40 cm focal length.

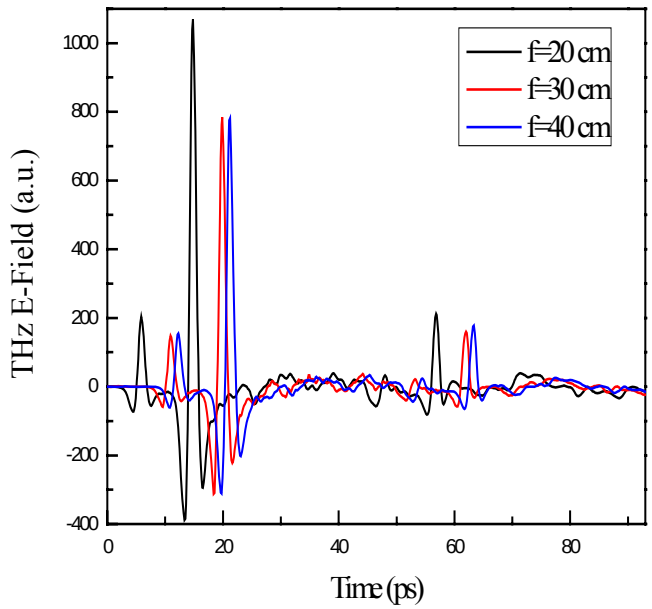

Figure 3.12: Terahertz waveform obtained by using lenses having 20 cm, 30 cm and 40 cm focal lengths.

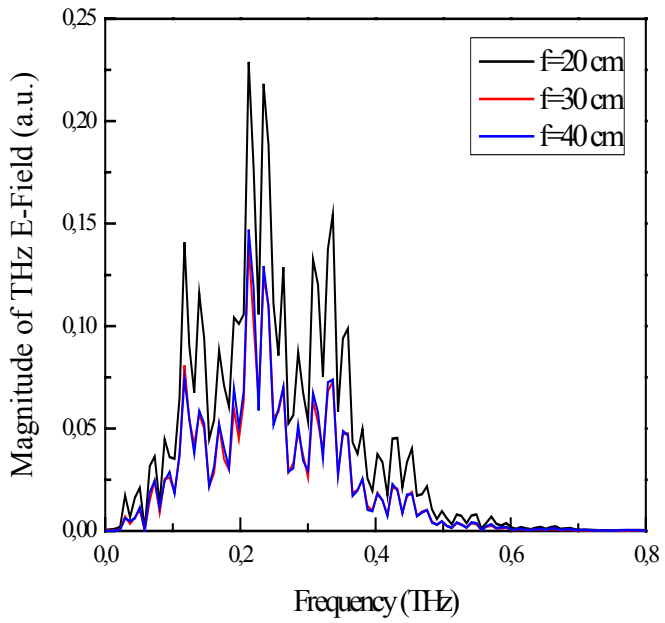

Figure 3.13: Magnitude of terahertz electric field obtained by using lenss having 20 cm, 30 cm and 40 cm focal lengths.

The relationship between the detected THz power and focal length of the lens used in the system is shown in the figure 3.14. The figure points out that there is a proportional relationship between the detected terahertz power and focal length of the lens used.

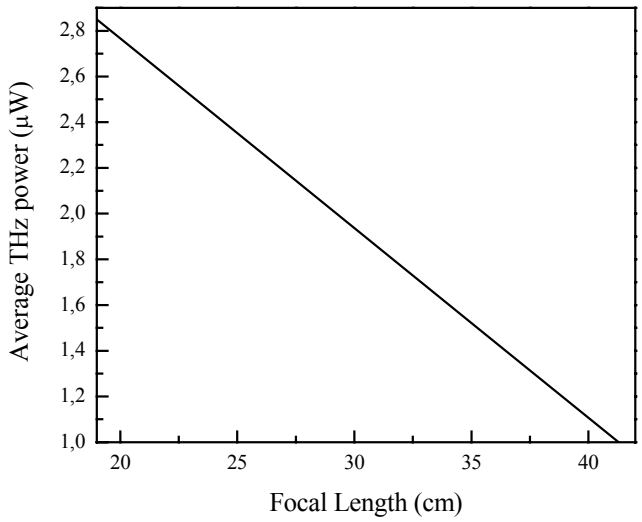

Figure 3.14: Average terahertz power versus focal length graph.

To further explore this effect confocal parameters of the probe beam on terahertz intensity profile were calculated. The beam parameters are listed as

ρ: radial distance from the center axis of the beam
z: the axial distance from the beam's narrowest point
I: intensity of the beam
w(z): width of the beam
w_0: the waist size
z_0: Rayleigh range
b: confocal parameter or depth of focus

d_{in}: entrance diameter

d_{out}: exit diameter

Firstly, the exit diameter of the terahertz beam is calculated with using the following formula,

$$d_{out} = f\theta = \frac{1.22\lambda}{d_{in}} \tag{3.55}$$

Half of the output diameter is gives the waist size of the beam. Next the axial distance from the beam's narrowest point is found by using the waist size with the following formula,

$$w_R = \frac{\pi w_0^2}{\lambda} \tag{3.56}$$

Finally multiplying this formula with two gives the confocal parameter of the beam. These calculations were made for the terahertz beam and all three cases of the probe beam as in the experimental study. Enterance diameter of the probe beam and terahertz beam were 2 mm and 6.34 mm respectively. Confocal parameters of the probe beam were calculated three times for different focal length values of the lens used in the system and resulting parameters were found to be 18.70 mm, 42.08 mm and 74.82 mm for lenses having focal lengths 20 cm, 30 cm and 40 cm respectively. In addition, depth of focus of terahertz beam was obtained as 2.5 mm at the exit of the parabolic mirror. This suggests that the focusing effects are purely due to the size of the spot rather than the divergence of the beam through the crystal since the crystal thickness was 2 mm, much less than the confocal parameters as calculated for the probe beam using the respective lenses. When the depth of focus values of probe beam are individually compared with that of the terahertz beam considering respective terahertz power, it is obivious that as the spot size of the probe beam

approaches that of the terahertz beam, detected terahertz power increases linearly.

3.3.2 THEORETICAL ANALYSIS

In this section effect of confocal parameters of the probe beam on the intensity profile of the terahertz beam was theoretically analyzed. In order to construct the intensity profile of the terahertz beam, we calculated the fraction of the intensities I/I_0 that occurs at $z = 0$ or $z/z_0 = 0$. It is calculated by the following formula,

$$\frac{I(\rho,0)}{I_0} = \exp\left[-\frac{2\rho^2}{w^2(z)}\right] \tag{3.57}$$

Consequently, obtained values of the fractional of power terahertz beam for the parabolic mirror with 11.68 cm focal length are 0.135 while for probe beam with lenses having 20 cm, 30cm, 40 cm focal lengths are 0.961, 0.914 and 0.853 respectively. By using the fractional intensity of the terahertz beam and assuming a gaussian beam profile, intensity profile for the terahertz beam was plotted in figure 3.13. Then the fractional intensities of the probe beam were localized on this intensity profile. It is observed that they were localized in the linear part of the intensity profile of the terahertz beam that is shown in figure 3.14. This indicates that as the fractional intensity of the probe beam increases, intensity of the terahertz beam increases proportionally. The spot size of the probe beam is inversely proportional to its fractional intensity and spot size diameters are 97.6 μm, 146.4 μm and 195.2 μm for the fractional intensities of 0.961, 0.914 and 0.853 respectively. Therefore we inferred that there is inversely proportional relationship between the spot size of the probe beam and intensity of the terahertz beam. Since intensity of the probe beam is directly related to its power, we concluded that as the spot size of the probe beam decreases power of the terahertz beam increases proportionally. Considering the experimental and theoretical results, we concluded that there is a proportional relationship between the spot size of the probe beam and the detected terahertz power.

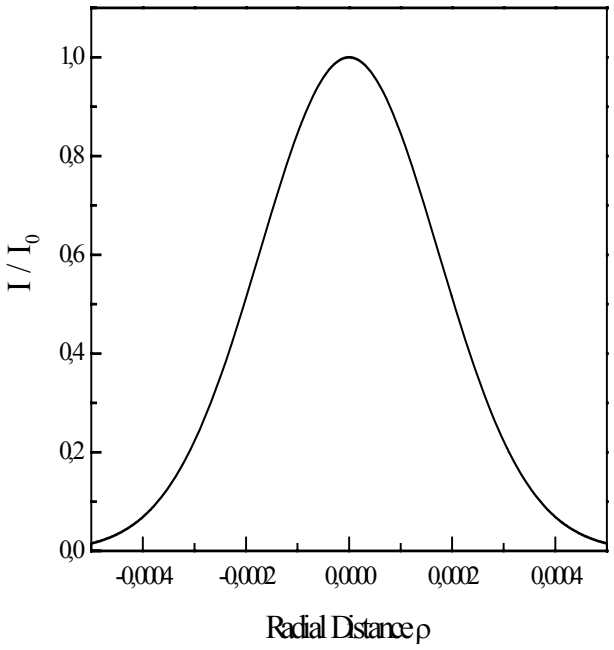

Figure 3.15: Intensity profile of terahertz.

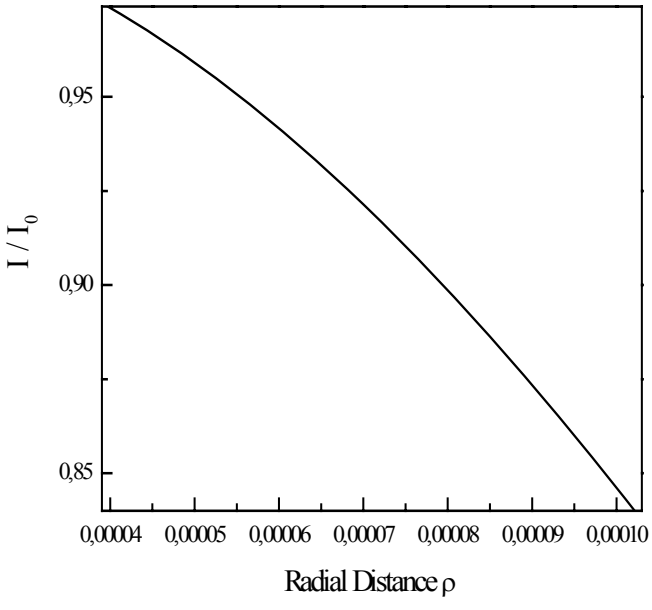

Figure 3.16: Fraction of intensities on the intensity profile of terahertz beam versus radial distance.

CHAPTER 4

CONCLUSION

The aim of this thesis was to design and construct a compact terahertz time-domain spectrometer. Hence in this work development of compact terahertz time-domain spectrometer was described. Several terahertz generation and detection methods were mentioned in chapter one with emphasis on electro-optic detection method. On the other hand, in chapter two, experimental aspects of the terahertz time-domain spectrometer including design and analysis for GaSe crystal were discussed. In addition, in chapter three characterization of detected terahertz power using electro-optic detection method was covered. As a result, a simple equation for the detected terahertz power was derived. We found that the measured THz average power was on the order of microwatts (~2.84μW) when photoconductive antennas were used for generation, which is consistent with previous literature measurements [63, 90-91]. Furthermore, influence of the spot size of the probe beam on the detected terahertz power was investigated by analyzing and comparing the terahertz power detected by electro-optic detection method with different focal spot size diameter of probe beam obtained by using different focal length focusing lenses. We observed that the detected THz power for the following lens focal lengths, 20 cm, 30cm, and 40 cm was 2.84 μW, 1.79 μW and 1.18 μW respectively. Our results suggest that the power detected by electro-optic detection method is enhanced for smaller spot size diameters of the probe beam, agreeing with out theoretical model which suggests that the peak THz power is at the center of the focused spot. As a result, we concluded

that there is a proportional relationship between the detected THz power and confocal spot size of the probe beam.

In conclusion, THz time-domain spectrometer based on electro-optic detection was built and an analysis was made with a GaSe crystal sample. In addition, the detected THz power was formulated and how it can be measured in such a system was analyzed. We found that the measured THz average power was on the order of few microwatts when photoconductive antennas were used for terahertz generation. Moreover, it was found that the probe beam should be focused onto the detection crystal to not only a spot size smaller than the THz beam diameter to obtain the highest detected THz power but also as small as possible to increase the detection sensitivity.

REFERENCES

[1]- R. H. Clothier & N. Bourne, "Effects of THz Exposure on Human Primary Keratinocyte Differentiation and Viability", J. Biol. Phys. 29, 179 (2003)

[2]- J. S. Olshevskaya, A. S. Ratushnyak, A K. Petrov, A. S. Kozlov & T. A. Zapara, "Effect of Terahertz Electromagnetic Waves on Neuron Systems", IEEE Region sbircon 8, 210 (2008)

[3]- M. G. Hauser & E. Dwek, "The Cosmetic Infrared Background: Measurement and Implications", Ann. Rev. Astronomy and Astrophysics, 39, 249 (2001)

[4]- M. Kimmit, "Restrahlen to T-Rays-100 Years of Terahertz Radiation", J. Biol. Phys. 29, 77 (2003)

[5]- E. R. Brown, K. A. Mclintosh, K. B. Nichols & C. L. Dennis, "Photomixing up to 3.8 THz in Low Temperature Grown GaAs", Appl. Phys. Lett. 66, 285 (1995)

[6]- T. Hidaka, S. Matsuura, M. Tani & K. Sakai, "CW Terahertz Wave Generation by Photomixing using a Two-Longitudinal-Mode Laser Diode", Elec. Lett. 33, 2039 (1997)

[7]- D. Saeedkia, A. H. Majedi, S. S-Naeini & R. R. Mansour, "Analysis and Design of a Photoconductive Integrated Photomixer/Antenna for Terahertz Applications", IEEE J. Quant. Elec. 41, 234 (2005)

[8]- G. P. Gallerano & S. Biedron, "Overview of Terahertz Radiation Sources", Proceedings of the 2004 FEL Conference (2004)

[9]- G. P. Williams, "Far-IR/THz Radiation from the Jefferson Laboratory, Energy Recovered Linac, Free Electron Laser", Rew. Sci. Inst. 73, 1461, (2002)

[10]- G. L. Carr, M. C. Martin, W. R. McKinney, K. Jordan, G. R. Neil & G. P. Williams, "High-Power Terahertz Radiation from Relativistic Electrons", Nature 420, 153 (2002)

[11]- M. Inguscio, G. Moruzzi, K. M. Evenson & D. A. Jennings, “A Review of Frequency Measurements of Optically Pumped Lasers from 0.1 to 8 THz”, J. Appl. Phys. 60, 161 (1986)

[12]- R. Köhler, A. Tredicucci, F. Beltram, H. E. Beere, E. H. Linfield, A. G. Davies, D. A. Ritchie, R. C. Lotti & F. Rossi, “Terahertz Semiconductor Heterostructure Laser”, Nature 417, 156 (2002)

[13]- S. Kumar, B. S. Williams, S. Kohen, Q. Hu & J. L. Reno, “Continious-Wave Operation of Terahertz Quantum Cascade Lasers Above Liquid Nitrogen Temperature”, Appl. Phys. Lett. 84, 2494 (2004)

[14]- S. Barbieri, J. Alton, H. E. Beere, J. Fowler, E. H. Linfield & D. A. Ritchie, “2.9 THz Quantum Cascade Lasers Operating up to 70 K in Continuous Wave”, Appl. Phys. Lett. 85, 1674 (2004)

[15]- S. Kumar, B. S. Williams, Q. Hu & J. L. Reno, “1.9 THz Quantum Cascade Lasers with One-Well Injector”, Appl. Phys. Lett. 88, 121123 (2006)

[16]- F. Lewen, R. Gendriesch, I. Pak, D. G. Paveliev, M. Hepp, R. Schieder & G. Winnewisser, “Phase Locked Backward Wave Oscillator Pulsed Beam Spectrometer in the Submilimeter Wave Range”, Rev. Sci. Inst. 69, 32 (1998)

[17]- P. R. Smith, D. H. Auston & M. C. Nuss, “Subpicosecond Photoconducting Dipole Antennas”, IEEE J. Quant. Elec. 24, 255 (1988)

[18]- B. B. Hu, J. T. Darrow, X. –C. Zhang, D. H. Auston & P. R. Smith, ”Optically Steerable Photoconducting Antennas”, Appl. Phys. Lett. 56, 886 (1990)

[19]- P. U. Jepsen, R. H. Jacobsen & S. R. Keiding, “Generation and Detection of Terahertz Pulses from Biased Semiconductor Antennas”, J. Opt. Soc. Am. B 13, 2424 (1996)

[20]- D. H. Auston, K. P. Cheung, J. A. Valdmanis & D. A. Kleinman, “Cherenkov Radiation from Femtosecond Optical Pulses in Electro-Optic Media”, Phys. Rev. Lett.53, 1555 (1984)

[21]- B. B. Hu, X. –C. Zhang, D. H. Auston & P. R. Smith, “Free-Space Radiation from Electro-Optic Crystals”, Appl. Phys. Lett. 56, 506 (1990)

[22]- L. Xu, X. –C. Zhang & D. H. Auston, “Terahertz Beam Generation by Femtosecond Optical Pulses in Electro-Optic Materials”, Appl. Phys. Lett. 61, 1784 (1992)

[23]- A. Rice, Y. Jin, X. F. Ma, X. –C. Zhang, D. Bliss, J. Larkin & M. Alexander, “Terahertz Optical Rectification from <110> Zinc-blende Crystals”, Appl. Phys. Lett. 64, 1324 (1994)

[24]- R. A. Kaindl, F. Eickemeyer, M. Woerner & T. Elsaesser, “Broadband Phase-matched Difference Frequency Mixing of Femtosecond Pulses in GaSe: Experiment and Theory”, Appl. Phys. Lett. 75, 1060 (1999)

[25]- T. J. Carrig, G. Rodriguez, T. S. Clement & K. R. Stewart, “Generation of Terahertz Radiation Using Electro-Optic Cystal Mosaics”, Appl. Phys. Lett. 66, 10 (1995)

[26]- A. Nahata, D. H. Auston, C. Wu & J. T. Yardley, “Generation of Terahertz Radiation from a Poled Polymer”, Appl. Phys. Lett. 67, 1358 (1995)

[27]- E. Budiarto, “Near-Field Propagation of Terahertz Pulses from a Large Aperture Antenna”, Opt. Lett. 23, 213 (1998)

[28]- D. H. Auston, K. P. Cheung, P. R. Smith, “Picosecond Photoconducting Hertzian Dipoles”, Appl. Phys. Lett. 45, 284 (1984)

[29]- Z. Wang, “Generation of Terahertz Radiation via Nonlinear Optical Methods”, IEEE Trans. on Geoscience and remote sensing 1,1 (2005)

[30]- M. Bass, P. A. Franken, J. F. Ward & G. Weinreich, “Optical Rectification”, Phys. Rev. Lett.9, 446 (1962)

[31]- W. Shi & Y. J. Ding, “Tunable Coherent Radiation from Terahertz to Microwave by Mixing Two Infrared Frequencies in a 47 mm Long GaSe Crystal”, International J. of high speed electronics and systems, 16, 589 (2006)

[32]- V. Y. Gaivoronsky, M. M. Nazarov, D. A. Sapozhnikov, E. V. Shepelyavyi, S. A. Shekelnyuk, A. P. Shkurinov & A. V. Shuaev, “Competition Between Linear and Nonlinear Processes During Generation of Pulsed Terahertz Radiation in ZnTe Crystal”, Quantum Electronics 35, 407 (2005)

[33]- R. Huber, A. Brodschelm, F. Tauser & A. Leitenstorfer, “Generation and Field-Resolved Detection of Femtosecond Electromagnetic Pulses Tunable up to 41 THz”, Appl. Phys. Lett. 76, 3191 (2000)

[34]- A. Nahata, A. S. Weiling & T. F. Heinz, “A Wideband Coherent Terahertz Spectroscopy System using Optical Rectification and Electro-Optic Sampling”, Appl. Phys. Lett. 69, 2321 (1996)

[35]- Q. Wu & X. –C. Zhang, “7 Terahertz Broadband GaP Electro-Optic Sensor”, Appl. Phys. Lett. 70, 1784 (1997)

[36]- A. Bonvalet, M. Joffre, J. L. Martin & A. Migus, “Generation of Ultrabroadband Femtosecond Pulses in the Mid-Infrared by Optical Rectification of 15 fs Light Pulses at 100 MHz Repetation Rate”, Appl. Phys. Lett. 67, 2907 (1995)

[37]- N. Katzenellenbogen & D. Grischowsky, “Efficient Generation of 380 fs Pulses of THz Radiation by Ultrafast Laser Pulse Excitation of a Biased Metal-Semiconductor Interface”, Appl. Phsy. Lett. 58, 222 (1991)

[38]- H. G. Roskos, M. C. Nuss, J. Shah, K. Leo, D. Miller, A. Fox, S. Schmitt-Rink & K. Köhler, “Coherent Submilimeter-Wave Emission from Charge Oscillations in a Double-Well Potential”, Phys. Rev. Lett.68, 2216 (1992)

[39]- A. V. Kuznetsov & C. J. Stanton, “Theory of Coherent Phonon Oscillations in Semiconductors”, Phys. Rev. Lett.73, 3243 (1994)

[40]- T. Dekorsy, H. Auser, C. Waschke, H. J. Bakker, H. G. Roskos, H. Kurz, V. Wagner & P. Grosse, “Emission of Submilimeter Electromagnetic Waves by Coherent Phonons”, Phys. Rev. Lett.74, 738 (1995)

[41]- P. Y. Yu & M. Cardona, “Fundamentals of Semiconductors: Physics and Material Properties”, 3rd Ed., Springer, pp. 110-113

[42]- T. Dekorsy, H. Auser, H. J. Bakker, H. G. Roskos & H. Kurz, “THz Electromagnetic Emission by Coherent Infrared-Active Phonons”, Phys. Rev. Lett. B 73, 4005 (1996)

[43]- A. Leitenstorfer, S. Hunsche, J. Schah, M. C. Nuss & W. H. Knox, "Femtosecond Charge Transport in Polar Semiconductors", Phys. Rev. Lett.82, 5140 (1999)

[44]- M. Tani, R. Fukasawa, H. Abe, S. Matsuura, K. Sakai & S. Nakashima, "Terahertz Radiation from Coherent Phonons Excited in Semiconductors", J. Appl. Phys. 83, 2473 (1998)

[45]- P. Gu, M. Tani, K. Sakai & T. –R. Yang, "Detection of Terahertz Radiation from Logitudinal Optical Phonon-Plasmon Coupling Modes in InSb Film Using an Ultrabroadband Photoconductive Antenna", Appl. Phys. Lett. 77, 1798 (2000).

[46]- S. L. Chuang, S. S. Rink, B. I. Greene, P. N. Saeta & A. F. J. Levi, "Optical Rectification in Semiconductor Surfaces", Phys. Rev. Lett.68, 102 (1992)

[47]- P. Gu, M. Tani, S. Kono, K. Sakai & X. –C. Zhang, "Study of Terahertz Radiation from InAs and InSb", J. Appl. Phys. 91, 5533 (2002)

[48]- K. Sakai, "Terahertz Optoelectronics", Springer Press, pp. 12-13

[49]- S. Kono, P. Gu, M. Tani & K. Sakai, "Temperature Dependence of Terahertz Radiation from n-type InSb and n-type InAs Surfaces", Appl. Phys. B. 71, 901 (2000)

[50]- H. Takahashi, A. Quema, R. Yoshioka, S. Ono & N. Sarukura, "Excitation Fluence Dependence of Terahertz Radiation Mechanism from Femtosecond-Laser-Irradiated InAs under Magnetic Field", Appl. Phys. Lett. 83, 1068 (2003)

[51]- H. G. Roskos, M. C. Nuss, J. Shah, K. Leo, D. Miller, A. Fox, S. Schmitt-Rink & K. Köhler, "Coherent Submilimeter-Wave Emission from Charge Oscillations in a Double-Well Potential", Phys. Rev. Lett.68, 2216 (1992)

[52]- P. C. M. Planken, M. C. Nuss, I. Brener, K. W. Goossen, M. S. C. Luo & S. L. Chuang, "Terahertz Emission in Single Quantum Wells After Coherent Optical Excitation of Light Hole and Heavy Hole Excitons", Phys. Rev. Lett. 69, 3800 (1992)

[53]- M. Hangyo, S. Tomozawa, Y. Murakami, M. Tonoichi, M. Tani, Z. Wang, K. Sakai & S. Nakashima, "Terahertz Radiation from Superconducting $YBa_2Cu_3Y_{7-\delta}$ Thin films Excited by Femtosecond Optical Pulses", Appl. Phys. Lett. 69, 2122 (1996)

[54]- Y. Konishi, M. Kamegawa, M. Case, R. Yu, M. J. W. Rodwell, R. A. York & D. B. Rutledge, "Picosecond Electrical Spectroscopy using Monolithic GaAs Circuits", Appl. Phys. Lett. 61, 2829 (1992)

[55]- S. Kono, M. Tani & K. Sakai, "Ultrabroadband Photoconductive Detection: Comparison with Free Space Electro-Optic Sampling", Appl. Phys. Lett. 79, 898 (2001)

[56]- P. L. Richards, "Bolometers for Infrared and Milimeter Waves", J. Appl. Phys. Lett: 76, 1 (1994)

[57]- M. Exter & D. R. Grischkowsky, "Characterization of an Optoelectronic Terahertz Beam System", IEEE Trans. Microwave Theory and Tech. 38, 1684 (1990)

[58]- Q. Wu & X. –C. Zhang, "Free Space Electro-Optic Sampling of Terahertz Beams", Appl. Phys. Lett. 67, 3523 (1995)

[59]- A. Yariv, "Quantum Electronics", Chapter 5, 3rd Ed. John Wiley & Sons Press

[60]- S. Dexheimer, "Terahertz Spectroscopy: Principles and Applications", CRC Press 2007, p. 47

[61]- P. C. M. Planken, H. Nienhuys, H. J. Bakker & T. Wenckebach, "Measurement and Calculation of the Orientation Dependence of Terahertz Pulse Detection in ZnTe", J. Opt. Soc. Am. B 18, 313 (2001)

[62]- H. J. Baker, G. C. Cho, H. Kurz, Q. Wu & X. –C. Zhang, "Distortion of Terahertz Pulses in Electro-Optic Sampling", J. Opt. Soc. Am. B., 15, 1795, (1998)

[63]- Q. Wu & X. –C. Zhang, "Design and Characterization of Travelling-Wave Terahertz Electro-Optic Sensors", J. Select. Topics Quantum Electron, 2, 693, (1996)

[64]- D. Liu & J. Qin, "Dependence of THz Time-Domain Spectroscopy on the Crystal Thickness and Optical Width in Electro-Optic Sampling", Int. J. Infrared and submilimeter waves, 24, 929, (2003)

[65]- D. M. Mittleman, R. H. Jacobsen, R. Neelemani, R. G. Baraniuk & M. C. Nuss, "Gas Sensing Using Terahertz Time-Domain Spectroscopy", Appl. Phys. B 67, 379 (1998)

[66]- P. Kuzel & J. Petzelt, "Time Resolved Terahertz Transmission Spectroscopy of Dielectrics", Ferroelectrics, 239, 949 (2000)

[67]- T. Jeon & D. Grichkowsky, "Characterization of Optically Dense, Doped Semiconductors by Reflection THz Time Domain Spectroscopy", Appl. Phys. Lett. 72, 3032 (1998)

[68]- I. Wilke, M. Khazan, C. T. Rieck, P. Kuzel & T. Kaiser, "Terahertz Surface Resistance of High Temperature Conducting Thin Films", J. Appl. Phys. 87, 2984 (2000)

[69]- S. D. Brorson, R. Buhleier, I. E. Trofimov, J. O. White, C. Ludwig, F.F. Balakirev, H. U. Habermeiner & J. Kuhl, "Rlectrodynamics of High Temperature Superconductors with Coherent Terahertz Pulse Spectroscopy", J. Opt. Soc. Am. B 13, 1979 (1996)

[70]- M. B. Campbell & E. J. Heilweil, "Non-Invaisive Detection of Weapons of Mass Destruction Using THz Radiation", SPIE Proc. 5070 (2003)

[71]- F. Huang, B. Schulkin & H. Altan, "Terahertz Study of 1,3,5-trinitro-s-triazine by Time-Domain and Fourier Transform Infrared Spectroscopy", Appl. Phys. Lett. 85, 5535 (2004)

[72]- H. Zhang, A. Redo-Sanchez & X. –C. Zhang, "Standoff Sensing and Imaging of Explosive Related Chemical and Bio-Chemical Materials Using THz-TDS", Selected topics in electronics and systems Vol. 49: Terahertz science and technology for military and security applications, pp.47-57, World Scientific 2007

[73]- J. Chen, Y. Chen, H. Zhao, G. J. Bastiaans & X. –C. Zhang, "Absorption Coefficients of Selected Explosives and Related Compounds in the Range of 0.1-2.8 THz", Optics Express 15, 12060 (2007)

[74]- R. M. Woodward, W. P. Wallace, R. J. Pye, B. E. Cole, D. D. Arnone, E. H. Linfield & M. Pepper, "Terahertz Pulse Imaging of Ex Vivo Basal Cell Carcinoma", J. Inves. Derma. 120, 72 (2003)

[75]- E. Pickwell, B. E. Cole, A. J. Fitzgerald, M. Pepper & V. P. Wallace, "In Vivo Study of Human Skin Using Pulsed Terahertz Radiation", Phys. Med. Biol. 49, 1595 (2004)

[76]- Y. C. Sim, I. Maeng & J. Son, "Frequency-Dependent Characteristics of Terahertz Radiation on the Enamel and Dentin of Human Teeth", Current Appl. Phys. 9, 946 (2009)

[77]- A. G. Markelz, A. Roitberg & E. J. Heilweil, "Pulsed Terahertz Spectroscopy of DNA, Bonvine Serum Albumin and Collagen Between 0.1 and 2.0 THz", Chem. Phys. Lett. 320, 42, (2000)

[78]- M. Walther, B. Fisher, M. Schall, H. Helm & U. P. Jepsen, "Far-Infrared Vibrational Spectra of All Trans, 9-cis and 13-cis Retinal Measured by Terahertz Time Domain Spectroscopy", Chem. Phys. Lett. 332, 389, (2000)

[79]- B. M. Fischer, M. Walther & P. U. Jepsen, "Far-Infrared Vibrational Modes of DNA Components Studied by Terahertz Time Domain Spectroscopy", Phys. Med. Biol. 47, 3807 (2002)

[80]- T. R. Globus, D. L. Woolard, T. Khromova, T. W. Crowe, M. Bykhovskaia, B. L. Gelmont, J. Hesler & A. C. Samuels, "THz-Spectroscopy of Biological Molecules", J. Biol. Phys. 29, 89 (2003)

[81]- M. Walther, P. Plochocka, B. Fisher, H. Helm & P. U. Jepsen, "Collective Vibrational Modes in Biological Molecules Investigated by Terahertz Time-Domain Spectroscopy", Biopolymers 67, 310 (2002)

[82]- Q. Wu, T. D. Hewitt & X. –C. Zhang, "Two-Dimensional Electro-Optic Imaging of THz Beams", Appl. Phys. Lett. 69, 1026 (1996)

[83]- Femto Lasers, “User’s Manual for Mirror Dispersion Controlled Ti:Sapphire Oscillator Femtosource”, Vienna, Femtosource Scientific (2004)

[84]- Batop Antennas, http://batop.de/products/PCA/pdf_sheets/PCA-44-06-10-800.pdf, last accessed date: 17 July 2009

[85]- K. Sakai, “Terahertz Optoelectronics”, Springer Press, pp. 7

[86]- J. Rudd & D. Mittleman, “Influence of Substrate-Lens Design in Terahertz Time-domain Spectroscopy”, J. Opt. Soc. Am. B 19, 319 (2002)

[87]- Batop Antennas, http://batop.de/products/overview/PCA1_flyer.pdf, last accessed date: 17 July 2009

[88]- T. Hattori, Y. Homma, A. Mitsuishi & M. Tacke, “Indices of Refraction of ZnS, ZnSe, ZnTe, CdS, and CdTe in the Far Infrared”, Opt. Commun. 7, 229 (1973)

[89]- N. C. J. Valk, T. Wenckebach & P. C. M. Planken, “Fulll Mathematical Description of Electro-Optic Detection in Optically Isotropic Crystals”, J. Opt. Soc. Am. B 21, 622 (2004)

[90]- M. Tani, S. Matsuura, K. Sakai & S. Nakashima, “Emission Characteristics of Photoconductive Antennas Based on Low-temperature-grown GaAs and Semi-insulating GaAs”, Appl. Opt. 36, 7853 (1997)

[91]- Y. Cai, I. Brener, J. Lopata, J. Wynn, L. Pfeiffer, J. B. Stark, Q. Wu, X. C. Zhang & J. F. Federici, “Coherent Terahertz Radiation Detection: Direct Comparison Between Free-Space Electro-optic Sampling and Antenna Detection”, Appl. Phys. Lett. Vol.73, No.4, 27 July 1998.